

TOPICAL REVIEW • OPEN ACCESS

## A review of label-free photonics-based techniques for cancer detection in the digestive and urinary systems

To cite this article: G Castro-Olvera *et al* 2025 *J. Phys. Photonics* **7** 012002

View the [article online](#) for updates and enhancements.

You may also like

- [1 GHz fundamental repetition rate thulium-doped all-polarization maintaining modelocked fiber laser](#)  
C Cuadrado-Laborde, H Muñoz-Marco, P Pérez-Millán *et al.*
- [Optical wavefront shaping in deep tissue using photoacoustic feedback](#)  
Fei Xia, Ivo Leite, Robert Prevedel *et al.*
- [Binary amplitude holograms for shaping complex light fields with digital micromirror devices](#)  
R Gutiérrez-Cuevas and S M Popoff



## TOPICAL REVIEW

## OPEN ACCESS




## A review of label-free photonics-based techniques for cancer detection in the digestive and urinary systems

RECEIVED  
6 May 2024REVISED  
19 August 2024ACCEPTED FOR PUBLICATION  
11 October 2024PUBLISHED  
22 November 2024

Original content from this work may be used under the terms of the [Creative Commons Attribution 4.0 licence](https://creativecommons.org/licenses/by/4.0/).

Any further distribution of this work must maintain attribution to the author(s) and the title of the work, journal citation and DOI.



G Castro-Olvera<sup>1,14,\*</sup> , E Baria<sup>2,3,14</sup>, D Stoliarov<sup>4,14</sup>, S Morselli<sup>5,6</sup>, B Orlandini<sup>7</sup>, M Vanoni<sup>8</sup>, H Sayinc<sup>9</sup>, A Koviarov<sup>4</sup> , D Galiakhmetova<sup>4</sup>, J Dickie<sup>10</sup>, R Cicchi<sup>2,3</sup>, S Serni<sup>5,6</sup>, M Gacci<sup>5,6</sup>, M J Ribal<sup>11</sup>, F S Pavone<sup>2,3,12</sup>, P Loza-Alvarez<sup>1</sup>, E Rafailov<sup>4</sup> and R Gumenyuk<sup>13</sup> 

<sup>1</sup> ICFO-Institut de Ciències Fòtoniques, The Barcelona Institute of Science and Technology, Barcelona 08860, Spain

<sup>2</sup> National Institute of Optics, National Research Council (CNR-INO), 50019 Sesto Fiorentino, Italy

<sup>3</sup> LENS—European Laboratory for Non-linear Spectroscopy, 50019 Sesto Fiorentino, Italy

<sup>4</sup> Aston Institute of Photonic Technologies (AIPT), Aston University, Birmingham, United Kingdom

<sup>5</sup> Unit of Urological Minimally Invasive and Robotic Surgery and Kidney Transplantation, Careggi University Hospital, Florence, Italy

<sup>6</sup> Department of Experimental and Clinical Medicine, University of Florence, Florence, Italy

<sup>7</sup> Unit of Gastroenterology, Careggi University Hospital, Florence, Italy

<sup>8</sup> Department of Biotechnology and Biosciences, University of Milano Bicocca and ISBE-Italy/SYSBIO, Milan, Italy

<sup>9</sup> LEONI Fiber Optics GmbH, 96524 Föritzal, Germany

<sup>10</sup> Modus Research and Innovation, Dundee, United Kingdom

<sup>11</sup> Department of Urology, Hospital Clinic, University of Barcelona, Barcelona, Spain

<sup>12</sup> Department of Physics, University of Florence, 50019 Sesto Fiorentino, Italy

<sup>13</sup> Laboratory of Photonics, Tampere University, Tampere, Finland

<sup>14</sup> These authors contributed equally.

\* Author to whom any correspondence should be addressed.

E-mail: [gustavo.castro@icfo.eu](mailto:gustavo.castro@icfo.eu)

**Keywords:** label-free, cancer diagnostic, SHG, Raman, TPEF, microscopy

## Abstract

For a long time, it has been known that optics can provide a broad range of tools for addressing clinical needs, particularly diagnostics. Optical techniques can help in identifying diseases and detecting pathological tissues with non/minimally invasive and label-free methods. Given the current limitations of standard clinical procedures, such an approach could provide a powerful tool in detecting gastrointestinal and bladder cancers. However, each technique has serious limitations regarding one or more of the following features: biomarker sensitivity, penetration depth, acquisition times, or adaptation to the clinical environment. Hence there is an increasing need for approaches and instruments based on the concept of multimodality; in this regard, we review the application of different imaging/spectroscopy tools and methods operating in the first two optical windows (SHG, SPEF, TPEF, THG, 3PEF, CARS, Raman and reflectance) for tumour detection in the digestive and urinary systems. This article also explores the possibility of exploiting the third bio-tissue transmission window (1600–1900 nm) by reviewing state of the art in ultrafast laser sources development. Finally, we summarize the most recent results in developing multiphoton endoscopes—a key element for clinical *in vivo* translation of photonics-based diagnostics.

## 1. Introduction and clinical needs

In 2020 more than 4 million cancer cases were diagnosed in Europe, and the most commonly diagnosed cancers were the following: breast, colorectal, prostate, lung and bladder cancers [1]. Compared to the 3.5 million cases from 2012, cancer incidence is clearly on the rise, and by 2040, the global number of new cancers per year is expected to rise to 29.5 million worldwide, including over 5 million in Europe alone [2, 3]. Many risk factors contributed to such increase, including ageing populations, pollution, and occupational risks. Colorectal and bladder cancers experienced a particularly strong increase in their incidence rates, a trend that is likely to continue in the next decade. Thus, improvements in detection and treatments are greatly advocated [4–6]. The standard diagnostic test for detecting bladder tumours is white light imaging

(WLI). However, this technique is burdened by false negatives and false positives at a non-negligible rate [7], as many endoscopic procedures can yield a high rate of false negative [8, 9]. Other techniques require fluorescent labels, such as aminolevulinic acid or fluorescein, but are not routinely used in clinical practice, due to their high cost and marginal improvement concerning WLI [10, 11].

In this framework, the introduction of new optical imaging techniques and related systems into the clinics have the potential to enhance the diagnostic power and the amplitude of their expanding biomedical applications, especially when implemented in a label-free modality. In fact, avoiding the administration of exogenous agents to the patient is a particularly crucial aspect for translating such promising technologies into clinical practice. For example, multimodal spectroscopy has already proved its potential in bladder cancer detection [12, 13]. In addition, modern laser sources allow developing new imaging techniques [14, 15] with the capability of reaching deeper areas of the examined tissue, avoiding tissue staining/labeling, potentially providing more information on the intrinsic content of the examined organs when compared to previous techniques.

A major obstacle to thoroughly appreciate current developments and future directions in this research area is the diverse nature of biological, clinical and technical challenges concurrently involved in tumour detection, as well as of these innovative technologies. Despite the relevance and interconnection of such topics, no attempt—to our knowledge—has been made to address them together in a comprehensive work. Therefore, given the rising interest for new optical methodologies and their possible application in the biomedical field, this article aims to provide an exhaustive review of the currently available label-free photonics-based techniques in cancer detection, with particular attention to those applied for urinary and colorectal cancers diagnostics. The information summarized in this work will hopefully help a broad range of clinicians and researchers in better understanding the capabilities and technical challenges of novel optical modalities and of the light sources involved in their use.

## 2. Current state-of-the-art of urological and gastrointestinal cancers detection

### 2.1. Clinically established techniques

Current applications of optical techniques in urologic and gastrointestinal cancer diagnostics are many and different. The most clinically established techniques for urologic and gastrointestinal cancer are WLI, narrow-band imaging (NBI) and photodynamic diagnosis (PDD) [16, 17]. WLI consists in shining a white light inside the patient through an endoscope or cystoscope. This well-established procedure helps doctors in visually assessing the presence of irregularities and suspicious areas. However, this technique provides small contrast for identifying specific types of bladder tumours, such as papillary lesions and carcinoma *in situ* hence causing higher recurrence-rates.

The further technical improvement led to NBI. NBI technology filters white light into two narrow bands (415 nm and 540 nm) that are efficiently absorbed by haemoglobin, increasing the visibility of surface capillaries and blood vessels in the submucosa. As carcinomas are highly vascularized, NBI enhances the contrast between superficial tumours and normal mucosa. Furthermore, studies conducted on bladder cancer have demonstrated that NBI is capable of detecting cancer areas more effectively than WLI [18, 19]. In fact, the endoscopes/cystoscopes currently available with this technology allow switching from one narrow band to the other by simply pushing a button on the instrument. On the other hand, technical improvements were also made in visualization and image enhancement, for example, Storz Professional Image Enhancement System have different visualization modules. Each visualization mode provides different color contrast, which varies according to a clinical situation (i.e. haematuria) or surgeons' preferences [20], allowing better visualization of the mucosa than WLI in different modalities.

PDD consists of the intravesical administration of precursors of the heme biosynthesis pathway. In fact, protoporphyrin IX, a precursor of heme, is photo-excitabile with emission in the red when excited using 400 nm wavelength. Nevertheless, *in vitro* studies demonstrated that urothelial neoplasms have a higher intake of these drugs [21]. Another photosensitizing agent is the 5-Aminolevulinic Acid. This is captured by cells with increased metabolic activity and can be excited using blue light in the 375–440 nm range. The precursors, that absorb the excitation light, emit a red light, which provides a contrast enhancement compared to WLI. This technique was firstly reported by Hörtl *et al* as an experimental *in vivo* and *in vitro* treatment and has been proved to be viable and effective to highlight urothelial cancer during cystoscopy [22]. Subsequent studies reported good outcomes also in association with another photosensitizer, Hexaminolevulinat, which proved superior in detection rate to WLI [18]. However, the use of endogenous contrast agents does not allow this technique to be a routine technique; even in some cases, it is possible that contrast media are not used due to the risk of adverse reactions.

## 2.2. Alternative techniques in cancer detection

Confocal laser endomicroscopy (CLE) is an optical imaging technique where a focused laser beam is scanning point by point to create a three-dimensional image; normally, a low-power blue laser for exciting fluorescence [23] is used. Exogenous fluorescence agents can be administered either topically or systemically [24] to directly perform a pathological exam of the tissues without taking a biopsy [25, 26]. This technique currently it is applied *in vivo*, especially in upper urinary tract urothelial cancer detection [26–28]. In a recently published systematic review and meta-analysis, CLE showed a good sensitivity and specificity in the detection of dysplasia in Barrett's oesophagus, gastric neoplasms and polyps, colorectal cancers in inflammatory bowel disease, malignant pancreatobiliary structures, and pancreatic cysts [29]. The main limitation of CLE is the fact that it needs for either topical or intravenous fluorescent agents. In addition to this, the technique is not widely available and need of specific training, it is of high cost and still there is a lack of comparison studies with other advanced optical techniques [23, 29].

Autofluorescence imaging (AFI) is another tool for cancer detection through fluorescence excitation. Differently from CLE, it does not use exogenous agents, hence a detailed description of its characteristics will be found in section 3 among the other label-free techniques.

## 2.3. Unmet clinical needs

Respect to WLI, the alternative technologies already available to clinicians do not provide—all things considered—the improvements required for replacing current gold standard procedures in the detection of urological/gastric tumours. Relatively high costs, low sensitivity to certain types of tumours, artefacts from exogenous agents, and operator-dependent analysis are the most important shortcomings that still affect the methodologies presented in this section. Therefore, there is still an unmet need for fast, reliable and economically sound systems to improve urothelial and gastrointestinal cancer management both for clinicians and for patients.

On the other hand, recent systems employing novel photonics-based technologies—multiphoton and spectroscopy imaging—are currently under development, and seems to provide good results *ex-vivo* [12–14]. These techniques can provide immediate, high contrast by analyzing the intrinsic morphochemical content of tissues, especially when implemented in a multimodal approach. In this regard, the following sections will discuss the characteristics of label-free photonics-based techniques and their application to diagnosing cancer in both the digestive and urinary systems.

Currently available clinical techniques have different limitations. The lack of contrast makes the diagnosis strongly dependent on the clinicians' experience, which makes the results and interpretations susceptible to human error. On the other hand, although these techniques have shown great sensitivity in detecting cancer in its advanced stages, this has not been the case for early stages. The limited depth of penetration, as well as the need for not using contrast agents, has prompted research and the development of novel methodology and instruments for urologic and gastrointestinal cancers detection.

## 3. Emerging label-free optical techniques of urologic and gastrointestinal cancers detection

In the presence of incident light beam, several optical processes can occur at the same time. In inhomogeneous materials such as biological tissues, the different optical properties of each structure can produce different light-matter interactions, often resulting in different contrast mechanisms that can be exploited for tissue imaging. In this review, we have addressed 4 main types of optical techniques in label-free modality: reflectance, autofluorescence, Raman spectroscopy, and multiphoton microscopy (MPM).

### 3.1. Optical reflectance

Reflectance (elastic back scattering) is a simple and label-free technique that has been applied to both spectroscopy and imaging fields. A common implementation consists of illuminating the sample with a broadband source (e.g. a halogen or LED lamp) and collecting the reflected light. This approach allows investigating the scattering and absorption properties of the target and has been used for monitoring the presence of known absorbers within body tissues, such as haemoglobin, melanin and water [30]. WLI and NBI are clear examples of reflectance-based techniques.

### 3.2. AFI

AFI has been recently developed to take advantage of the differences in tissue fluorescence properties of normal and neoplastic tissues that are generated by their endogenous fluorophores [31–34]. Narrow-band sources (such as lasers, diodes, and arc-lamps) can be used to excite endogenous autofluorescent molecules to higher energy states [35]. Biological tissues contain intrinsic fluorescent molecules, whose electronic

transitions can be typically excited using ultraviolet (UV) or near-UV light: nicotinamide adenine dinucleotide (NADH), flavin adenine dinucleotide (FAD), collagen, elastin, lipo-pigments, porphyrins, etc [36, 37]. Although fluorescent labels (such as the photosensitizing agents described in section 2) are already used in the clinical practice, there are several advantages for adopting autofluorescence as label-free contrast mechanism for imaging biological tissues: the abundance of endogenous fluorophores and their relationship to metabolic activities, relatively high acquisition speed, and the possibility to use low-power light sources [38].

During cystoscopy, for example, normal tissue mucosa imaged with AFI typically shows a green color, whereas an inflammatory or neoplastic lesion typically presents lower fluorescence intensity and appears brown-reddish or magenta. The potential detection efficacy of AFI for neoplasms lesion remains controversial though, as the use of UV or near UV limits diagnosis to only superficial layers, limited tissue samples have been studied to date, and a high level of skill is required, which may lead to misdiagnosis and low inter-observer agreement [39].

### 3.3. Raman spectroscopy

The Raman signal can be used to identify both organic and inorganic molecules, opening a wide range of possible applications for industrial and clinical purposes. This is based on measuring the rotational-vibrational spectrum of a molecule, which is highly related to its geometry, especially in the so-called fingerprint region ( $300\text{--}1900\text{ cm}^{-1}$ ). Therefore, a substance can be identified by observing its spectrum in such a region. There are two complementary optical techniques to do so: infrared (IR) absorption spectroscopy and Raman spectroscopy. The first is related to the interaction of IR light with the medium (absorption, emission or reflection) and in general, provides information on the vibrational states of matter. The latter is based on the Raman effect, i.e. the inelastic scattering of light after colliding with a molecule: the molecule undergoes a transition to a higher/lower rotational-vibrational energy state, causing the incident photon to lose/gain energy and to be scattered with a lower/higher frequency (Stokes/anti-Stokes Raman shift). Being independent of the excitation wavelength, this technique allows measuring the molecular rotational-vibrational transitions using either visible ( $380\text{--}700\text{ nm}$ ) or NIR ( $700\text{--}2500\text{ nm}$ ) laser light. However, the probability of Raman scattering is extremely low and, for biological tissues, the intensity of the Raman signal is several orders of magnitude smaller than the excited fluorescence emission. Consequently, the signal must be integrated for relatively long times, making such a technique typically used for imaging small areas. Nevertheless, the high specificity of Raman spectra has been successfully exploited for examining different body tissues, detecting and diagnosing many pathological conditions, including cancer [40, 41].

### 3.4. MPM

MPM techniques refer to those generated by the interaction of two, three or more photons. MPM, being a nonlinear effect, requires high intensities to produce an efficient light matter interaction [15]. Therefore, focusing beam is needed, generating a nonlinear effect only at the focal region. In MPM the signal is collected with a detector while the laser is scanned through the sample (as in a confocal microscope). For this reason, such approach can produce high-resolution, three-dimensional images [14]. Among the main multiphoton effects used are: second harmonic generation (SHG), third harmonic generation (THG), two-photon excited fluorescence (TPEF), three-photon excited fluorescence (3PEF), and Coherent Anti-stokes Raman Scattering (CARS), as shown in figure 1. Importantly, the efficiency of these nonlinear effects is based on their intrinsic material properties. This has the advantage that no exogenous agents (e.g. fluorescent labels) have to be added to gain contrast. However, since these effects depend on the sample structure, not every effect can be generated from a particular sample.

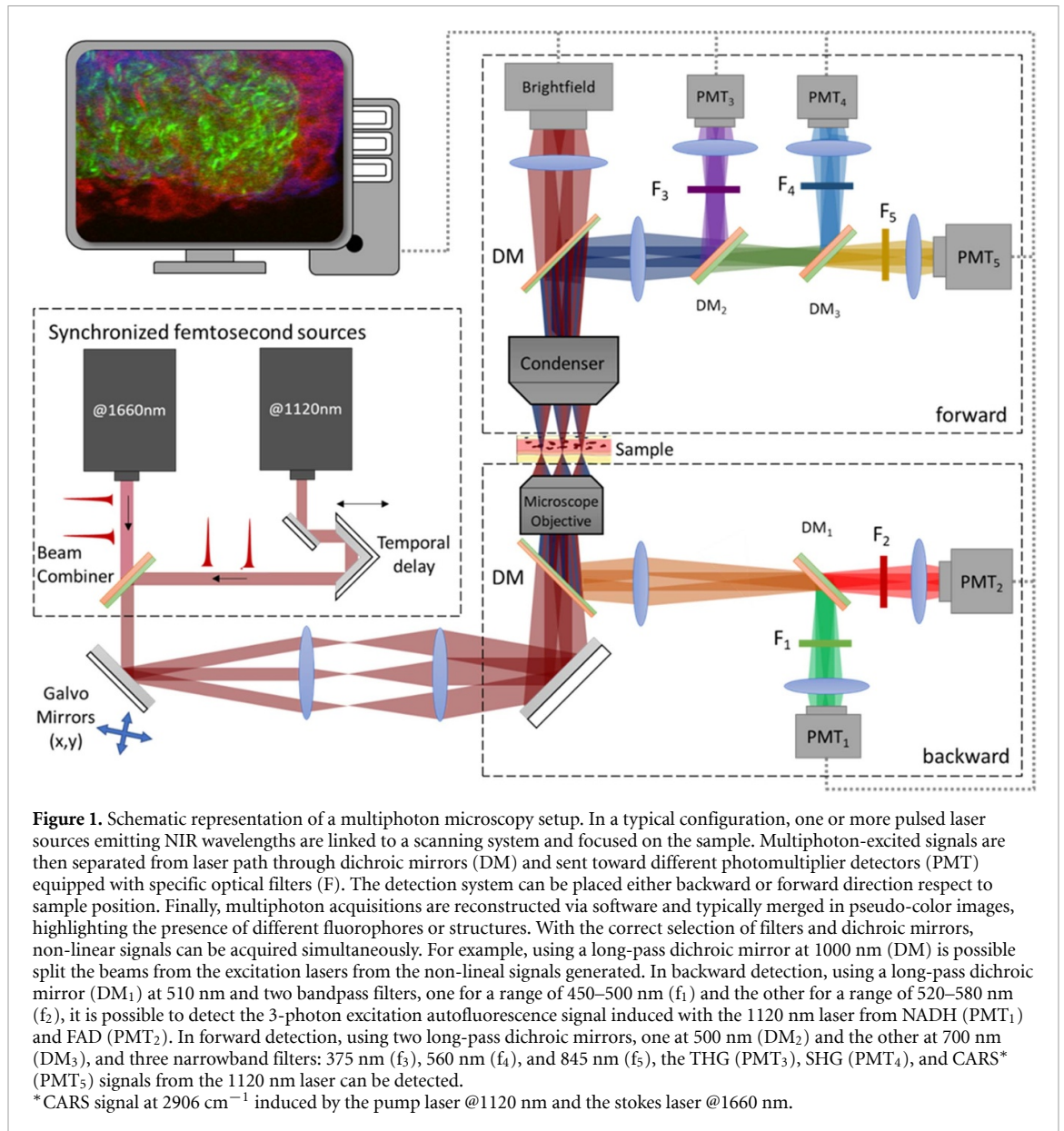
#### 3.4.1. SHG

SHG is a process in which two incident photons are transformed into one photon with an energy that is exactly equal to the sum of the excitation photons. In this case, the SHG signal is generated only when the laser pulse interacts with a non-centrosymmetric structure. Collagen [42–44], microtubules [45, 46], and myosin [47], among some others [44, 45, 48, 49], exhibit this type of crystal symmetry.

#### 3.4.2. THG

THG is a process that requires three photons to generate one at an energy three times the excitation photons. THG depends on the inhomogeneity of the medium, which makes the THG interface sensitive. Therefore, it is possible to use the THG signal as a contrast mechanism to identify any cellular interface [50] where there is a strong change in the refractive index.

Importantly, both SHG and THG techniques provide useful and complementary structural information about the tissue without the need to use any exogenous agent. As such, they present a huge potential for use



in diagnostic applications, although the excitation intensities required for their generation pose a higher risk of photodamaging tissues; this problem becomes more relevant as the nonlinearity of the optical process increases.

### 3.4.3. TPEF, 3PEF

TPEF is a process in which a molecule is excited to a higher electronic state by absorbing two low-energy photons, rather than a single high-energy photon as in conventional fluorescence. After excitation, the molecule returns to its ground state by emitting a fluorescence photon, which has higher energy than the photons of the excitation light. Similarly, 3PEF is a process that consists of the simultaneous absorption of three incident photons, followed by the emission of fluorescence. Contrary to linear fluorescence, only a small volume around to the focal region is excited, reducing the photo-bleaching effect to only this volume. This considerably reduces the phototoxic effects and increases the viability of the sample. In addition, due to the wavelength-dependence of scattering, longer excitation wavelengths can penetrate deeper than shorter ones, even in highly dispersive media such as biological tissues [51–56]. Due to the wide availability of visible fluorescent biomarkers that can be excited using ultrashort pulsed sources, TPEF has become one of the most widely used nonlinear microscopy techniques, while there is growing interest in 3PEF applications (such as deep imaging of scattering tissues like brain [57, 58]).

#### 3.4.4. Coherent Raman scattering (CRS)

CRS probes the same molecular transitions observable through spontaneous Raman spectroscopy, but in a much more efficient approach as it is based on stimulated emission. In fact, CRS techniques such as CARS and Stimulated Raman Scattering (SRS) need two synchronized lasers in order to induce a stimulated transition between rotational/vibrational levels, thus generating a signal which is orders of magnitude higher than the spontaneous process. In SRS, the target molecule is excited from the initial state toward a nearby rotational/vibrational level by two incident photons (a ‘pump’ and a ‘Stokes’ one), whose energy difference matches the separation between those levels. During such process, the SRS effect can be observed via changes in the Stokes beam intensity. Compared to SRS, in CARS the molecule is further excited toward a virtual level using another pump photon (‘probe’), and then the molecule relaxes to its ground state emitting a high-frequency photon—the CARS signal to be detected. These two CRS techniques can be used for label-free imaging based on specific Raman bands (typically) of lipids and proteins.

## 4. Advanced imaging technologies for cancer detection

### 4.1. Applications to cancer detection in the gastrointestinal system

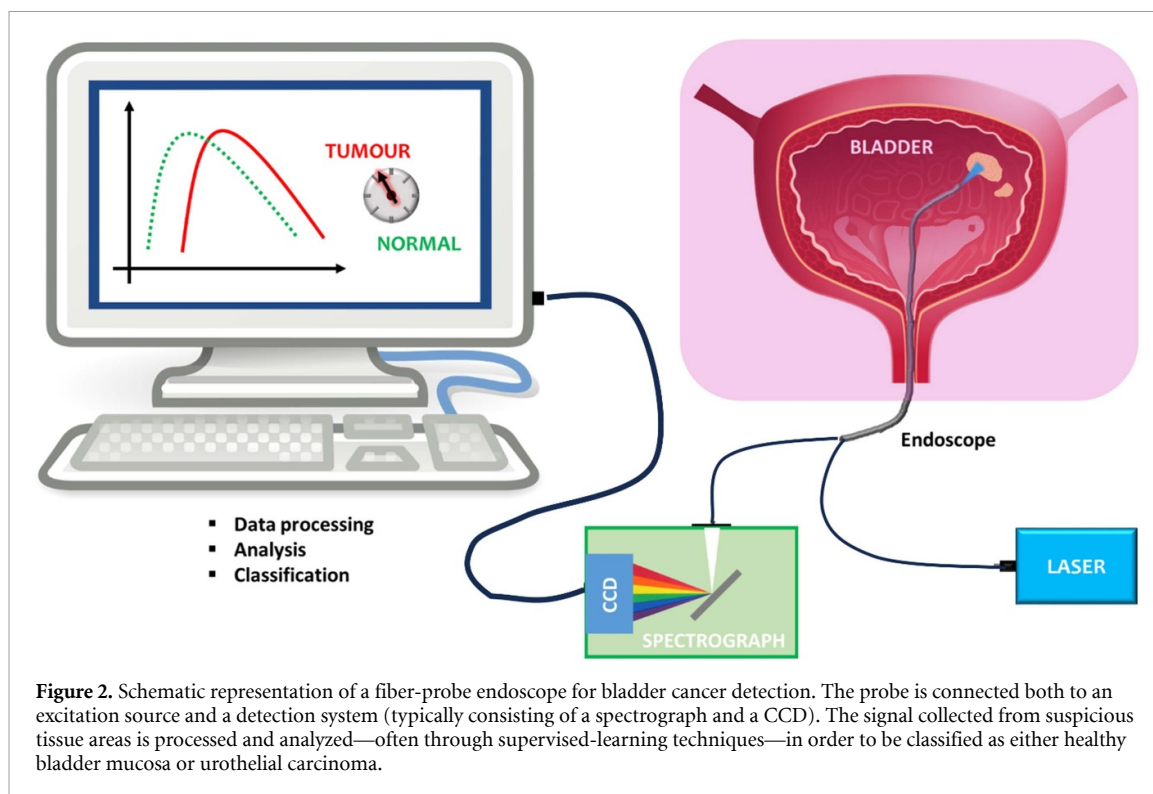
During the 1990s, studies on this subject involving autofluorescence [59–62] and optical reflectance techniques [63, 64] were published, showing their potential. During the 2000s, studies based on Raman spectroscopy [65–67] were also presented. A literature review (table A1 [59–62, 68–75], table A2 [63, 75–85] and table A3 [65–67, 73, 86–94] in the Annex section) suggests that these techniques could be successfully applied—both *in vivo* (through endoscopy) and *ex-vivo*—to the detection of gastrointestinal tumours. The research on the field continues to the present day.

A consensus is that neoplastic tissues in the gastrointestinal system are characterized by both lower absolute intensities in fluorescence emission and higher red-to-green ratio with respect to non-tumour areas [68, 71, 75, 95–97]. In fact, several factors have been cited to explain these effects in tumours: bigger cells, causing a reduction in collagen and elastin concentrations (which contribute to green fluorescent emission); thicker mucosa layer, screening off collagen/elastin emissions from the submucosa layer; higher concentration of non-fluorescent NAD<sup>+</sup> relative to fluorescent NADH; increased concentration of red-emitting porphyrins. Such features usually provide high sensitivity on average (~90%) in tumour detection, although there is great variability in reported sensitivities (table A1).

Another feature observed in a gastrointestinal tumour is angiogenesis, where resulting hypoxia and increased haemoglobin concentration can be probed through reflectance measurements [63, 81, 84, 85]. Moreover, several studies [75, 77, 79, 82–85] obtained better sensitivities and specificities by extending the analysis to longer wavelengths, above 900 nm, where fat, collagen and water are important chromophores. On average, the presented studies on reflectance-based endoscopy (table A2) obtained ~90% sensitivity and specificity.

Raman systems (mainly fiber-optic probes) were applied to study gastrointestinal tumours, providing important insights on the molecular composition and metabolic activity of such tissues. The analysis of tumour Raman spectra highlighted a reduction in glycogen [65, 98], collagen and lipids concentrations [87, 88], together with an increase in DNA contents [86, 90]. These findings are consistent with hallmarks of tumour development, including increased energy consumption from cell division, increased thickness of the gastric epithelial layer due to proliferation of the malignant cells and increased nuclear/cytoplasmic ratio. Almost all the studies reported in table A3 used NIR wavelengths and adopted supervised learning algorithms to differentiate tumour from non-tumour tissues with high sensitivity and specificity. Importantly, half of the studies reported in table A3 performed *in vivo* measurements, paving the way for clinical implementation, preferably in combination with the other two techniques.

In the digestive system, multiple research groups have focused on gastrointestinal cancer detection using non-linear optical methods, including SHG, THG, TPEF, 3PEF, CARS and SRS (table A4). Many focused their efforts on detecting SHG produced by collagen [51, 99–112]. As a result of these investigations, healthy and cancerous tissue can now be distinguished based on histological differences, using THG to distinguish the boundaries of different biological components (tissues, cells or cellular components) [113, 114]. Furthermore, autofluorescence has been used to identify the signals and distribution of FAD and NADH into the tissue using TPEF or 3PEF [51, 103, 110, 112]. Recently, this has been used to generate multiphoton images with a resolution comparable to histopathology [43, 108–114]. Nonlinear microscopy has proven to be a useful imaging tool for the qualitative and quantitative evaluation of various diseases. Furthermore, due to the nature of non-linear signals, it is possible to collect simultaneously structural (SHG, THG) and metabolic (TPEF, SRS, CARS) information from the tissue. All of this can be done with minimal phototoxicity to tissues, at depths of several hundred microns with the ability to detect cellular and subcellular microstructures of tissues [108, 111, 112]. Due to these advantages, some research groups have



focused on gastrointestinal cancer detection using multiphoton techniques. Most of these investigations use biopsies from different parts of the gastrointestinal tract. However, some investigations have taken these techniques to an intraoperative level and have been able to distinguish between healthy tissue and gastric carcinoma *in-situ* and *in vivo* [51, 99, 100, 113].

#### 4.2. Applications to cancer detection in the urinary system

During the 1990s, several studies investigated the possibility of using tissue autofluorescence for detecting bladder tumours, beginning with *in vivo* measurements through a bifurcated fiber-bundle inserted into a cystoscope (figure 2), observing that tumour areas show an average decrease in NADH and collagen fluorescence intensity with respect to normal bladder mucosa [115]. Later studies, for both *in vivo* [116–119] and *ex vivo* [120, 121], adopted similar approaches (based on fiber-optic probes) and confirmed these results. Moreover, tryptophan, FAD and porphyrins were found to be other major fluorophores involved, and UV excitation wavelengths (<400 nm) were found to be more effective [120, 121] in discriminating normal and tumour tissues. Finally, the research suggested that collagen and NADH emissions are reduced by thickening the urothelial layer in tumours [120, 121], which prevents the detection of autofluorescence coming from deeper layers (i.e. from collagen in the lamina propria and NADH in muscle layers).

The observed spectral changes, including a spectral redshift in tumour peak intensity [12, 13, 118], were used for discriminating neoplastic tissues from the normal bladder. The most common approach consisted in calculating the ratio between fluorescence intensities detected at two separated wavelengths, but two studies [12, 13] adopted a method based on Principal Component Analysis (PCA), a well-known statistical tool for multivariate analysis. Table A5 summarizes the major findings of the above-mentioned studies. Tumours were detected on average with ~90% sensitivity and specificity, despite variation from differing experimental conditions (number of patients and samples, excitation wavelength, data analysis, instrumentation, etc). Hence, autofluorescence spectroscopy appears as an effective tool for improving the detection of bladder tumours during cystoscopy.

*In vivo* studies [122, 123] examined bladder tumours through another technique: reflectance spectroscopy. Using broadband excitation sources (such as halogen or xenon lamps) and collecting the reflected light upon large spectral ranges (~hundreds of nm), normal and neoplastic tissues' absorption and scattering properties were investigated. Mourant *et al* [122] developed a classification method based on the spectral slope recorded in the 330–370 nm range. Koenig *et al* [123] analyzed longer wavelengths to probe the total amount of haemoglobin (hence, of blood), which they found to be higher in tumours. This finding was also observed by Slaton *et al* [124], and appears to reflect tumour angiogenesis, i.e. a higher microvessel density in neoplastic tissues with respect to the healthy bladder. Such features were later exploited for the



implementation of NBI in bladder tumour detection. By filtering both excitations and reflected light signals within two narrow bands, centred on major haemoglobin absorption peaks (415 nm and 540 nm), it is possible to enhance the contrast between well-vascularized lesions and normal mucosa. This technique can be implemented in video cystoscopes and used for real-time imaging of the bladder. For example, Rosenzweig *et al* [125] listed 12 *in vivo* studies comparing NBI to standard white-light cystoscopy, of whom we included in table A6 those with >100 patients [126–129]. Another feature for differentiating normal bladder from cancer may be the slope of reflectance spectra recorded between 600 and 700 nm [13]: being proportional to the average size of light scatterers, such parameter could highlight the presence of tumour cell nuclei, as (on average) they are bigger than normal ones.

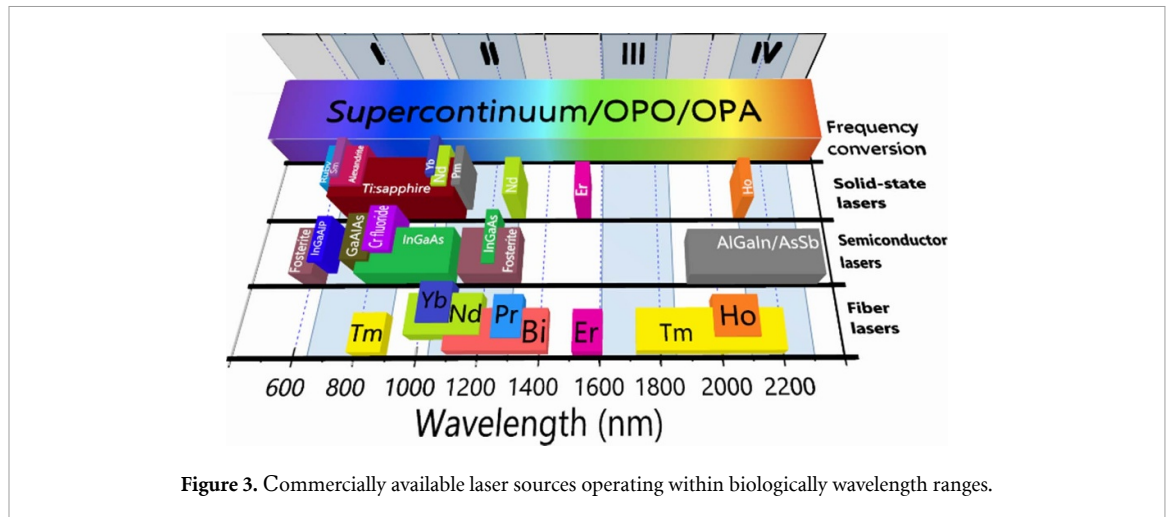
In general, tumour identification through reflectance-based methods is characterized by high sensitivity (up to 100%), whereas specificity values fluctuate mostly between 60% and 80%. However, results from spectroscopic [12, 13, 122–124] and NBI studies are difficult to be compared: the former is based on objective parameters extracted from the spectra, while the latter are based on ‘the physician’s ability to identify tumours as well as to other subjective factors’ [129]. Another important difference between the two approaches is that fiber-optic devices used in spectroscopy require scanning the probe along with each point of the examined tissue area, whereas all pixels of the NBI image are recorded simultaneously, allowing faster acquisitions.

Both fluorescence and reflectance have been successfully employed for detecting intrinsic differences in the composition of benign and malignant bladder areas. In this regard, Raman spectroscopy could provide an additional and more detailed characterization, being able to probe molecular content of these tissues. The first attempts came in the early 2000s from Stone *et al* [65] and Crow *et al* [130], with both groups obtaining very high sensitivity (>97%) and specificity (>93%) in discriminating bladder cancer. These studies paved the way for developing and applying Raman fiber-optic probes to the same biomedical problem, resulting in many independent papers [12, 13, 131–136] that validated the previous results. Table A7 lists the Raman literature on the field. Most of the reported works shares common features, such as employing fiber-probes, adopting NIR excitation wavelengths (785 nm being the most common), and analyzing the recorded dataset through a combination of PCA and linear classification models (mainly Linear Discriminant Analysis). Moreover, there is general agreement about the interpretation of Raman spectra: compared to healthy mucosa, decreasing collagen content and an increasing presence of lipids, amino acids and DNA were observed in cancer spectra [12, 132, 134, 135, 137], reflecting the altered metabolism of tumour tissues.

On average, Raman spectroscopy/microscopy obtained ~90% sensitivity and specificity in detecting bladder tumours. Notably, there is smaller variability between the results of Raman papers than among the fluorescence literature on the same subject. However, all but one [132] of the studies reported in table A7 were conducted *ex-vivo*. In fact, the main challenge in using Raman-based methods is their relatively long integration time: recording a spectrum typically required 10–20 s in the reported literature, which is several orders of magnitude higher than in fluorescence/reflectance-based techniques. This is a clear obstacle for *in vivo* implementation in the clinical setting.

On the other hand, Raman spectroscopy has also been applied for differentiating bladder tumour grades (table A8) by exploiting its higher molecular specificity with respect to other techniques. Such a task can be performed after tissue excision, hence measurements requiring a few tens of seconds or minutes would pose no effective delay nor an obstacle to standard clinical routines. The known literature reports 89% sensitivity and 83% specificity, on average, in discriminating low-grade (LG) from high-grade (HG) bladder tumours. Efforts were also made to differentiate bladder tumour stages, such as  $T_a$  (non-invasive),  $T_1$  (connective-tissue-invading) and  $T_2$  (muscle-invading) urothelial carcinomas [12, 13, 130, 132]. The results obtained in differentiating  $T_a$  from the two invasive stages range between 96% sensitivity/96% specificity obtained in Crow *et al* [130] and 41% sensitivity/83% specificity in Draga *et al* [132]. Raman spectroscopy could play an important role in examining freshly excised tissue biopsies and providing an automated diagnosis of bladder tumours, which would help in designing a proper medical treatment immediately after cystoscopy.

As with gastrointestinal cancer, ongoing work uses MPM to detect bladder cancer (table A9 [138–143]). To date, most applications using MPM are limited to biopsies. There are various approaches to collecting and discerning this information. The most explored way is collecting the SHG produced by collagen fibers. By comparing collagen fibers morphology, several studies have been able to differentiate between healthy bladder tissue and carcinoma [138–144]. It is also possible to take advantage of the information of autofluorescence induced by the absorption of two or three photons of molecules whose absorption is in the UV region including NADH, keratins, melanin, and elastin. Since these techniques induce the fluorescence of endogenous tissue molecules, different spectral analyses can be incorporated into the signals in order to differentiate the molecules. One approach is to fix the sources of ultrashort pulses to the most efficient wavelength for each of the endogenous molecules and generate maps of the different signals of the tissue. It is



also possible to combine nonlinear techniques with techniques based on fluorescence lifetime, such as Fluorescence lifetime imaging Lifetime Imaging Microscopy (FLIM) or Spectral fluorescence Lifetime Imaging Microscopy to differentiate each endogenous molecules of the tissue [12, 139, 141]. With this, it has been possible to determine the distribution of the FAD and NADH molecules. In addition to this, with the structural information obtained by SHG collagen, notable differences have been demonstrated between the regions of healthy tissue and urothelial carcinoma [12, 138–141].

As previously mentioned, many studies have identified Raman spectrum peaks where there is greater variation between healthy tissue and urothelial carcinoma. They have taken advantage of Raman information to generate metabolic maps through the use of techniques such as CARS or SRS. Finally, there are more ambitious works that have managed to collect simultaneously the signal of TPEF, SHG and CARS and combine this information with the spectral information from TPEF-FLIM and Raman [142] to generate multimodal images contrasting morphological and metabolic characteristics between healthy tissue and cancer. Thus, research has demonstrated the ability of these modalities to provide diagnostic information, and their potential to become a diagnostic tool for detecting the disease in its early stages and improving the understanding of associated pathophysiological processes.

#### 4.3. Laser sources for optical diagnostics of the digestive and urinary systems

Optical reflectance techniques for tissue classification typically require the use of broadband light sources and optical filters in the emission and collection light paths. Fluorescence or Raman generation, instead, requires narrow-band, continuous wave laser sources, the most popular [145, 146] being semiconductor laser diodes.

Diverse categories of pulsed laser sources are used for the optimal functioning of MPM systems, contingent upon their specific applications. Consequently, determining the most suitable excitation light source for MPM of specific tissue types presents a complex challenge. Multiple parameters warrant consideration for an effective comparison, including but not limited to: image quality (comprising both blur and noise), sample safety, imaging depth, and the versatility of available imaging modes., etc [147]. Figure 3 depicts the emission wavelength ranges that most of the commercial lasers [148, 149].

Solid-state lasers employ a crystal or glass host material that is doped with specific ions such as Neodymium (Nd), Ytterbium (Yb), Chromium (Cr), or Titanium (Ti) to achieve the desired lasing wavelength. These lasers can operate across a broad spectrum, ranging from the visible to the near-infrared (NIR), typically between 0.5 and 1.6  $\mu\text{m}$  [150]. Semiconductor lasers function across an extensive wavelength spectrum, from UV to mid-infrared (MIR), partially encompassing the biological windows except for the third one. InGaAs, with a tunable direct bandgap, is ideal for specific wavelengths in biological windows, while GaAs is used for NIR lasers and AlGaInAsSb for lasers beyond 2  $\mu\text{m}$  in the MIR range [148]. In fiber lasers the active gain medium is doped with rare-earth elements such as Erbium (Er), Ytterbium (Yb), Thulium (Tm) and etc [149]. The operational wavelength range of fiber lasers is generally between 1  $\mu\text{m}$  and 2.2  $\mu\text{m}$ , although specialized designs and methods can extend this range. One such method is supercontinuum generation, which is produced by the propagation of intense laser pulses in a transparent nonlinear medium, resulting in ultra-broadband radiation. This radiation has a high power spectral density and a high degree of coherence, making it equivalent to a white-light laser [151].

In the context of MPM, the most used and explored source is the titanium-doped sapphire (Ti:Sapphire or ti:sapph) laser, as this can be used to excite nonlinearly most of the visible fluorescent markers. A high

**Table 1.** The list of biological windows. The bandwidth of each biological window is listed in the second column from the left. The wavelengths of nonlinear excitation (third column) and the generated signals for the case of SHG and THG are listed in the third and fourth columns, respectively.

Biological window	Wavelength range (nm)	Fundamental (nm)	SHG (nm)	THG (nm)
1st	700–950	825	412	275
2nd	1000–1350	1150	575	383
3rd	1600–1870	1700	850	566
4th	2100–2300	2200	1100	733

saturation energy, large stimulated emission cross-section, and broad absorption gain bandwidth make Ti:Sapphire the most successful solid-state laser material in the NIR wavelength range. They have excellent tunability in the range of 650–1100 nm and high potential for ultrashort pulses creation.

However, Ti:Sapphire lasers are generally confined to the laboratory. These lasers are not appropriate for industrial or mobile applications due to their temperature and vibration sensitivity. Furthermore, they are still massive, complex, high-priced [149]. In this context, cutting-edge fiber lasers are excellent alternative which could offer compactness, industrial reliability, power scalability, wide spectral working range and superior beam quality from the fiber output [152].

## 5. Complementary technologies for *in vivo* detection of bladder and gastrointestinal cancers and future

### 5.1. Multimodal multiphoton micro-endoscopes

*In vivo* implementation of multiphoton techniques—especially in a multimodal configuration—offers a promising tool for assessing the presence, grade and stage of tissue lesions like bladder/gastric tumours. Such task is currently carried out *ex-vivo*, i.e. through biopsy extraction and histopathological examination, but this procedure has some limitations: high cost, invasiveness, sampling errors, time-consumption and the inability to monitor the lesion. Multimodal Multiphoton Microscopy (MMM), on the other hand, could provide label-free, high-resolution optical sections of a few hundred micrometers below the tissue surface, without the need for collecting and staining biopsies, providing high-sensitivity 3D images with micrometer accuracy. Moreover, MMM could also be used for better defining tumour margins during surgical removal. However, the greatest challenge in the clinical translation of this technology is the difficulty in obtaining multiphoton images from internal organs, which requires the development of fully integrated multimodal microendoscopy systems (tables A10 and A11 [153–167]).

Currently, microendoscopy systems have been able to be fully integrated into probes of 3 mm in diameter and 4 cm in length [153–155] to satisfy the clinical requirements for use at the hospital level. These probes are made up of microelectromechanical mirrors or piezoelectric actuators [156], to control the position of the excitation laser. Furthermore, these probes are coupled to double-coated optical fibers [153–161], which allows the excitation and emission wavelengths to be transmitted efficiently.

However, translating multimodal microendoscopy to the clinic involves many technological challenges. It is essential that the microendoscope is small enough (i.e. less than 2 mm in diameter) to be inserted into a clinical endoscope [157–159]. Furthermore, for efficient multiphoton excitation it is necessary to deliver ultrashort IR pulses thorough to several meters long of optical fiber, with efficient dispersion management to ensure high peak powers at the end of the endoscope and without introducing distortions [162–167], whilst keeping the large field of view (FOV > 150  $\mu\text{m}$ ), the large working distance (WD > 1 mm) and the highest resolution possible (<1  $\mu\text{m}$ ). The development of this technology has been increasing progressively in recent years, making pulse transmission and detection more efficient. These advances in multimodal endoscopic imaging capabilities present numerous promising opportunities for applications in both clinical diagnostics and basic research, creating a tool for real-time gastrointestinal and bladder cancer diagnosis and treatment.

### 5.2. New technologies for deep tissue multiphoton imaging

To increase tissue penetration depth, efforts have been focused on using longer wavelengths, where scattering is minimized. Additionally, due to the high peak intensities required by the non-linear process, it is necessary to work in the so-called biological windows, where light absorption is minimal. Currently, there are four known wavelength regions, or biological windows [168], listed in table 1. Each biological window has a different transmission depending on the specific biological tissue [15, 153].

In biological terms one of the advantages of the ti:sapph laser is the most works in the first biological windows. Nevertheless, the generated nonlinear signal (TPEF, SHG, THG, etc.) are generated in the visible, far from an biological window. This will limit again the sample depth that can be examined through these

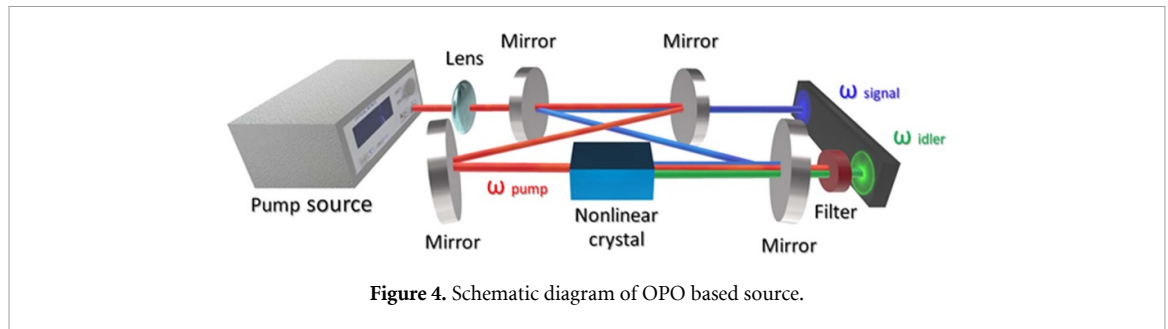


Figure 4. Schematic diagram of OPO based source.

techniques, as optical scattering will further reduce the intensity of the collected nonlinearly generated signal. On the other hand, the second biological window is being explored more and more due to the different commercially available laser sources (Ytterbium (Yb)-based laser). However, the non-linear signals are also produced in the visible range. Despite recent advancements in Tm and Ho ultrafast laser sources, the fourth biological window (2100–2300 nm) has been largely ignored. This is primarily due to the high water absorption in this wavelength range and the lack of high-sensitivity imaging detectors suitable for these wavelengths [169–173].

The potential of the third wavelength range of the biological window (1600–1870 nm) in multiphoton imaging remains largely unexplored, but it promises several advantages for working with deep tissues compared to the first and second transparency windows. Studies using 1700 nm excitation have demonstrated deep brain imaging experiments (signal-to-noise ratio (SNR) of  $\sim 5$  dB) and a penetration depth of 1.1 mm [174]. Similar results have been achieved in the urinary system, with a 1700 nm light source reaching a penetration depth of  $\sim 800 \mu\text{m}$  in normal prostate tissue [175]. As mentioned, the scattering decrease as the excitation wavelength increases. This means that less power is needed to reach the focus with longer-wavelength light, significantly increasing the penetration depth in tissues [174]. Additionally, the nonlinear features of multi-photon microscopy allow for minimizing out-of-focus light excitation and photobleaching of biological samples [176]. Considering the increased penetration depth and reduced effect of optical scattering, the use of these longer wavelengths for both excitation and emission are highly favorable for imaging systems [14]. Therefore, one of the most interesting regions is the third biological window; however, there are still no commercial femtosecond lasers in this region.

In this review, we focus on the two most popular techniques to achieve pulsed laser radiation in the 3rd biological window: optical parametric generators and pulsed fiber lasers.

### 5.2.1. Optical parametric generators and amplifiers

One of the most popular methods for generating laser sources emitting radiation in the third biological window is optical parametric generation. This approach offers a wide range of precisely tunable wavelengths with a high SNR, making it suitable for many applications including bio-imaging, time-resolved spectroscopy, chemical sensing, and microscopy [177–179]. Parametric light generation relies on the phenomenon where an incident photon in a nonlinear optical medium converts into two lower-energy photons, called the signal and idler waves. Their wavelengths are determined by the phase-matching condition and the principle of energy conservation. Phase-matching conditions can be changed by media temperature or, in bulk optics, by the angle between the incident pump beam and the crystal optical axes.

As a pump source, optical parametric oscillators (OPOs) are the primary approach of optical parametric light generation. Here, a nonlinear medium is placed in the cavity and the signal and the idler waves are built up from the noise using pump wave and cavity feedback (figure 4) [180]. O'Connor *et al* reported a synchronously pumped, periodically poled lithium niobate-based OPO with signal output tuned from 1550 to 1950 nm [181], obtaining up to 90 mW average power in a signal wave.

To increase the output power and improve the conversion efficiency, an optical parametric amplifier (OPA) with a low-power seed source is commonly used. OPOs acting as a seed source are widely applied in the OPA based sources of third biological window radiation [182]. For instance, Morz *et al* (2015) have demonstrated an optical parametric master oscillator power amplifier (MOPA), tunable from 1370 to 4120 nm [183]. For pumping, a Yb:KGW laser was used, which delivers up to 8 W average output power at 43 MHz repetition rate and 500 fs pulse duration at a central wavelength of 1030 nm. OPO and OPA were based on periodically-poled magnesium oxide doped congruent lithium niobate crystals. This system allows obtaining a high average power of up to 1.3 W at 1750 nm with 43 MHz repetition rate. OPO seed sources provide high pulse-to-pulse stability and SNR which positively affects bio-imaging. However, they have complex optical schemes and highly precision alignment requirements. To avoid these issues, SC sources are

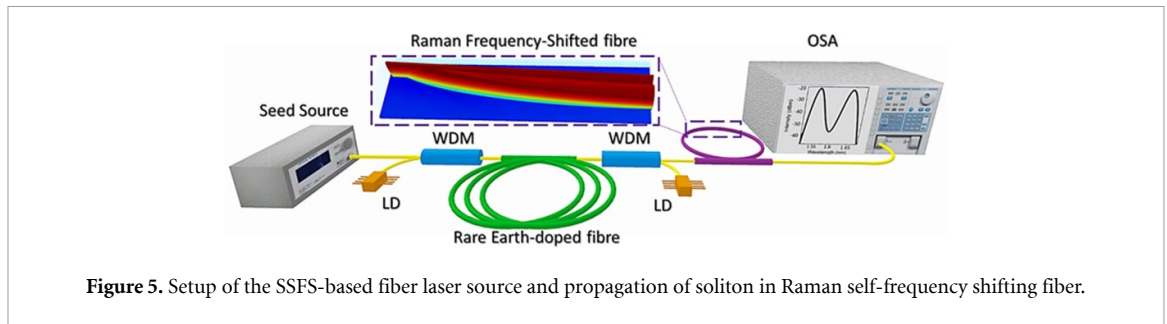


**Figure 5.** Setup of the SSFS-based fiber laser source and propagation of soliton in Raman self-frequency shifting fiber.

often used as an OPA seed [179, 184–186]. Optical parametric systems allow obtaining required laser radiation parameters at the third biological window, and they are capable of satisfying high requirements of bio-imaging but usually have a high cost, large footprint, and sensitivity to vibration. In fiber parametric oscillators (FOPO), these disadvantages are partially eliminated. Becheker *et al* demonstrated all fiber FOPO laser system at 1700 nm [187], obtaining 14.3 mW average power at 1700 nm. Power scaling in the FOPO system can be very difficult due to the nonlinear effects in optical fiber, keeping the output power less than 20 mW. To increase the output power, it is necessary to use optical parametric chirped-pulse amplifiers [188], which allows pulse amplification greater than 25 dB at 1550 nm [189]. With the correct fulfilment of the phase-matching condition, this approach makes it possible to get a wide-range wavelength-tunable fiber laser at 1700 nm [190]. Recently, a laser with a 450 fs pulse duration at 1700 nm and an average power of 1.41 W has been developed [191]. However, it features an extremely complex tuning mechanism and requires the use of specialized fibers. Well-known methods widely employ specialized fibers such as photonic crystal fibers (PCF), dispersion-shifted fibers (DSF), or highly nonlinear fibers for wavelength conversion and energy scaling purposes.

The OPO and OPA systems are attractive for bio-imaging due to high SNR and pulse-to-pulse stability. On the other hand, fiber lasers are great at working in harsh environments.

### 5.2.2. Ultra-short pulsed fiber lasers

The development of a highly stable, robust, compact, easy-to-use, and more affordable ultrashort pulse fiber laser has opened the door for MPM systems to be used in the clinical environment. The ultrafast rare-earth-doped fiber lasers are highly adaptable and more compact than many of their counterparts (figure 5). Furthermore, they offer simplicity of exploitation and reliability at working in harsh and inhospitable environments. Despite the fiber medium of lasers, the repetition rate of ultrashort fiber lasers could be adjusted in order to applications requirement by acousto-optic [192], applying piezo elements [193] or harmonic mode-locking methods [194, 195] with optical injection [196].

Recently, bismuth (Bi)-doped fibers have become popular as an active media of lasers. The main reason is the discovery of a broadband luminescence in the near IR region (1100–1800) nm in several Bi-doped glasses (silicate, germanate, aluminophosphate, barium-aluminoborate). The unique optical properties of Bi-doped fibers provide an opportunity to generate laser pulses in the broad spectral regions for various applications [197–201].

Using a high concentration of  $\text{GeO}_2$  and  $\text{SiO}_2$  in a Bi-doped fiber core, the emission spectral range could be extended to the wavelength region from 1.6 to 1.8  $\mu\text{m}$  [200]. The first 1.7  $\mu\text{m}$  Bi-doped fiber laser generating ultrashort pulses via passive mode-locking was demonstrated by Noronen *et al* in 2016 [201]. Later, the 630 fs pulse and output pulse energy of 5.7 nJ at 1.7  $\mu\text{m}$  were achieved in the Bi-doped fiber MOPA by Khagai *et al* [197]. Bi-doped fibers are an immature technology though and have a small core diameter ( $\sim 2 \mu\text{m}$ ), which leads to low pulse energy at the output and a requirement for a large cavity length due to the low gain per meter. The usage of Bi-doped fibers limits the fundamental pulse repetition rate up to 10 MHz in such lasers [200, 201].

Thulium (Tm)-doped fiber lasers operating at a wavelength of 1700 nm and longer, are more efficient than lasers based on Bi-doped fibers. A higher doping level of Tm in optical fibers allows shortening the cavity length and attaining higher energies. To investigate the expanding range of radiation tuning (1788–1831 nm and 1702–1764 nm) in a mode-locked fiber laser doped with Tm, Emami *et al* employed a specially designed PCF [202]. By relying on the partial amplified spontaneous emission suppression mechanism, which involved the combined use of two fabricated PCFs and the nonlinear polarization rotation method, the laser's emission wavelength band was effectively tuned. Advancements in the production of high-performance Tm-doped fibers enabled the development of a mode-locked fiber laser capable of generating ultrashort pulses in the wavelength range of 1700–1900 nm. Utilizing an

**Table 2.** Fiber laser systems emitting around 1700 nm.

Technology	Pulse duration (fs)	Pulse energy, (nJ)	References
FOPO	450	40	[169]
Bi-doped fiber MOPA	630	5.7	[175]
Tm-Ho	630	0.02	[179]
Er-doped & SSFS in SM telecom fiber	384	0.03	[201]
Er-doped & SSFS in DSF	196	0.7	[202]
Er-doped & SPM in DSF	85	10.6	[203]
Er-doped & SSFS in LMA	75	9	[204]
Er-doped & SSFS in LMA PCF	100	10	[205]
Er-doped & SSFS in PC rod	70–80	50–65	[206]

acousto-optical filter allowed for effective control of the spectral range within the cavity. The laser, combined with a Tm-doped fiber amplifier, produced pulses at 1708 nm with an energy of 1.85 nJ [203]. Nevertheless, the strong reabsorption at 1700 nm in Tm-doped fibers makes reaching high-performance laser sources at the shorter wavelengths highly difficult.

Erbium-doped fiber (EDF) has become the central component of nearly all optical amplifiers in the 1500–1600 nm spectral region. The most developed laser systems operating in this region are based on EDF, as EDF provides an efficient broad-band gain in the telecommunications window. The amplified spontaneous emission bandwidth of EDF does not cover the third optical window, although nonlinear effects in optical fibers can provide a frequency shift of EDF lasers. The self-phase modulation (SPM) [204] and cross-phase modulation [205], four-wave mixing [206], SRS [207, 208], and stimulated Brillouin scattering [209, 210] are all to play important roles in the creation of fiber lasers and amplifiers, signal format conversion and wavelength conversion devices [211]. These nonlinear effects are actively used in optical fibers to shift the spectral envelope of the pulse or generate new frequency components, including the generation of radiation in the third biological window.

Currently, several technologies are actively used to transfer energy from the Erbium emission wavelength (1500–1600 nm) to the range of the third biological window 1600–1870 nm, based on nonlinear effects in optical fiber. He *et al* demonstrated a compact laser with a pulse width of 384 fs and an average power of 35 mW with a conversion efficiency of about 60% using 460 m of standard single mode (SM) fiber telecom for a frequency shift of up to 1700 nm [212]. ZDW-shifted fibers are frequently employed in the implementation of both SPM and SSFS techniques, with the objective of attaining wavelengths in the range of 1650–1750 nm [213, 214].

Cadreas *et al* endeavored to enhance the output characteristics of radiation by devising a specialized fiber possessing a LMA. In conjunction with a cladding mode stripper and a band-pass filter employing soliton self-frequency shift, they achieved pulses with a 9 nJ energy, 75 fs duration, and a wavelength of 1650 nm [215]. Subsequent studies employing commercially available LMA fibers have demonstrated comparable conversion efficiencies [216]. In 2014 Wang *et al* presented the SSFS system based on photonic crystal rod (PC Rod) that could prove the pulse with energy >60 nJ [217]. However, they require much higher initial pump pulse energy, water cooling, and cannot be coiled. The progress in developing tunable ultra-short fiber pulsed lasers covering the third biological window gives the ability to choose the most appropriate laser parameters for deep and high-resolution imaging. Table 2 demonstrates the results achieved in generating ultrashort laser pulses at 1700 nm using various fiber laser schemes and techniques.

Latest developments in 1700 nm laser sources pave the way for 3PEF imaging in the third biological window and, potentially, its future application to cancer detection in the digestive and urinary systems. However, to be competitive with standard clinical procedures (see sections 1 and 2), an alternative methodology must meet some important requirements: high imaging speed, high label-free sensitivity/specificity, and deep tissue penetration.

Although no technique meets all needed criteria, their combination in a multimodal approach could overcome individual shortcomings and complement each other's information retrieved from the sample. In fact, nonlinear imaging methods can provide a high-resolution morphological characterization of the examined tissues, while spectroscopic methods allow probing their composition and metabolic activity. Such an approach could improve tumour detection and margins identification. Nonetheless, one major challenge in the clinical application of multimodal imaging remains the adaptation of multiphoton techniques to an endoscopic environment.

**Table 3.** List of advantages and disadvantages of major photonics-based techniques.

Technique	Advantages	Disadvantages
Autofluorescence	<ul style="list-style-type: none"> <li>• Fast imaging</li> <li>• Detection of intrinsic fluorophores<sup>a</sup></li> <li>• Allow spectroscopy analysis</li> </ul>	<ul style="list-style-type: none"> <li>• Low penetration depth</li> <li>• Limited molecular characterisation</li> </ul>
Reflectance	<ul style="list-style-type: none"> <li>• Fast imaging</li> <li>• Allow spectroscopy analysis</li> <li>• Simple Setup</li> </ul>	<ul style="list-style-type: none"> <li>• Low penetration depth</li> <li>• Limited molecular characterisation</li> </ul>
Raman	<ul style="list-style-type: none"> <li>• High-detailed molecular characterisation</li> <li>• Medium penetration depth</li> </ul>	<ul style="list-style-type: none"> <li>• Long integration time</li> </ul>
SHG	<ul style="list-style-type: none"> <li>• High spatial resolution</li> <li>• High penetration depth</li> <li>• Provide structure information for non-centrosymmetric molecules</li> </ul>	<ul style="list-style-type: none"> <li>• Non molecular identity</li> <li>• Directionality</li> <li>• Need a ultrashort source</li> </ul>
TPEF/3PEF	<ul style="list-style-type: none"> <li>• High spatial resolution</li> <li>• High penetration depth</li> <li>• Detection of intrinsic fluorophores<sup>a</sup></li> <li>• Allow spectroscopy analysis</li> </ul>	<ul style="list-style-type: none"> <li>• Only few fluorophores can be excited<sup>a</sup></li> <li>• Limited molecular characterization</li> <li>• Requires ultrashort source</li> </ul>
CARS	<ul style="list-style-type: none"> <li>• High spatial resolution</li> <li>• High penetration depth</li> </ul>	<ul style="list-style-type: none"> <li>• Limited molecular characterization</li> <li>• Directionality</li> <li>• Requires two ultrashort sources</li> <li>• Complex setup</li> </ul>
THG	<ul style="list-style-type: none"> <li>• High spatial resolution</li> <li>• High penetration depth</li> <li>• Provide structure information of interfaces and optical heterogeneities</li> </ul>	<ul style="list-style-type: none"> <li>• Non molecular identity</li> <li>• Directionality</li> <li>• Requires ultrashort source</li> </ul>

<sup>a</sup> The fluorophores that can be excited depend on the source spec (wavelength, broadband and time duration) available in the market.

## 6. Summary

Improving cancer detection, particularly in the digestive and urinary systems, constitutes a prominent objective for the future, especially in front of rising tumour incident rates and their associated costs. In order to evaluate the possibility of adding alternative tools to current clinical procedures, in this article we reviewed the relevant literature on the applications non-invasive optical methods (Raman, reflectance and autofluorescence, TPEF, SHG, THG, 3PEF, and CARS) to the study of gastrointestinal and urothelial tumours. Using these techniques, either in single modality or in a multimodal approach, many studies have already demonstrated the possibility to extract important morphochemical information from the label-free examination of both *ex-vivo* and *in vivo* tissues. In fact, the analysis of spectra and images acquired from unstained bladder/gastric samples has proved the ability to highlight and quantify significant differences in metabolic activity and properties of normal and diseased tissues, such as molecular composition, oxygenation and morphological features. These parameters could be used for automated, fast, operator-independent evaluation of suspicious tissue areas or biopsies, providing a useful tool to complement WLI.

However, clinical implementations of photonics-based techniques for detecting gastrointestinal and bladder cancers require the use of endoscopes adapted to such task. Well-established solutions are already available for spectroscopic and imaging applications of linear optical techniques; instead, endoscopes for multiphoton imaging face many technological challenges and are still under development (although some have been successfully tested).

On the other hand, scattering and water absorption constitute major obstacles for single-photon techniques when examining deep tissue layers, which is of paramount importance for assessing tumour infiltration and could also help in verifying safe margins during its surgical removal. In this context, 2- and (even more) 3-photon excitation techniques provide clear advantages in tissue penetration, optical resolution and reduced photodamage. And while the majority of reviewed papers implemented SHG/TPEF microscopes, the latest developments in ultrafast laser sources—in particular, emitting around 1700 nm—could pave the way for increased use of THG and 3PEF imaging. The third biological window promises several advantages for working with deep tissues for multiphoton imaging. In this regard, table 3 reports the advantages and disadvantages of all the techniques reviewed in this article.

Full exploitation of the possibilities offered by the photonics-based techniques summarized in this review requires correlating the performance of these techniques with an in-depth knowledge of the molecular and metabolic modifications connected with the observed spectroscopic and microscopic readouts. Suitable preclinical systems aimed at reconstructing the tumor microenvironment allow performing in-depth genetic and molecular analyses that are often impossible on clinical samples. These techniques include the growth of three-dimensional cultures of stabilized cell lines (spheroids) [218, 219] with varying degrees of aggressiveness and the production of organoids from clinical samples when sufficient bioptic material is available [220–222]. Some examples of the application of spectroscopic techniques on organoids and spheroids from tumors of the bladder and gastrointestinal tract have been published [223–230]. The integration of these spectroscopic analyses with molecular and post-genomic analyses will allow a more refined correlation of spectroscopic and biochemical properties, whose translation in the clinical setting may allow higher resolution patient staging, making it possible to design more effective and less toxic patient-specific personalized therapies [231, 232].

The implementation of label-free photonics-based techniques in the clinical environment represents an ambitious solution for increasing the diagnostic efficacy of current gold standard tests based on WLI. While each technique has strengths and weaknesses, their combination in a multimodal approach could overcome the individual shortcomings and significantly improve cancer diagnosis. A recent example of such efforts is represented by the European Union Horizon 2020 project called Advanced Multimodal Photonics Laser Imaging Tool for Urothelial Diagnosis in Endoscopy [14], which aims to analyze spheroids and organoids derived from bladder tumours through Raman, TPEF and 3PEF imaging, and to develop a multimodal endoscope (combining all three techniques) specifically designed for urothelial cancer diagnosis. More in general, the literature reviewed in this article suggests that photonics may play an ever-increasing role in translational research and, particularly, in detecting tumours in the digestive and urinary systems.

### Data availability statement

No new data were created or analyzed in this study.

### Acknowledgment

This project has received funding from the European Union's Horizon 2020 research and innovation programme under Grant Agreement No 871277 and is an initiative of the Photonics Public Private Partnership. G C O and P L A acknowledge funding from the Spanish Ministry of Economy and Competitiveness through the 'Severo Ochoa' program for Centres of Excellence in R&D (CEX2019-000910-S), from Fundació Privada Cellex, Fundació Mir-Puig, Generalitat de Catalunya through the CERCA program and Laserlab-Europe EU-H2020 (871124). RG acknowledges Research Council of Finland (320165). G C-O, E B and D S, contributed data analysis, manuscript preparation, writing and revising. A K and D G contributed to data analysis. All authors contributed to manuscript writing and revision. D J, R C, S M, E R, F S P, M V, P L A, R G contributed project conceptualization supervision and funding.

### Conflict of interest

The authors declare no competing interests.



## Annex

**Table A1.** List of studies reporting the detection of gastrointestinal tumours by fluorescence spectroscopy.

Paper	Year	Type	Patients <sup>a</sup> (N-T; T)	Sites <sup>a</sup> (N-T; T)	$\lambda_{exc}$ (nm)	Sens. (%)	Spec. (%)
Cothren et al [62]	1990	<i>in vivo</i>	20	67 (36; 31)		100	97
Kapadia et al [59]	1990	<i>ex-vivo</i>		70 (35; 35)	325	100	100
Marchesini et al [60]	1992	<i>ex-vivo</i>	45 (9; 36)	78 (42; 36)	410	80.6	90.5
Chwirot et al [61]	1997	<i>ex-vivo</i>	21	72 (50; 23)	325	96	52
Kobayashi et al [68]	2001	<i>in vivo</i>	52	54 (21; 33)	437	94	86
Mayinger et al [69]	2001	<i>in vivo</i>	13	129 (57; 72)	375–478	97	95
Xiao et al [70]	2002	<i>in vivo</i>	38 (21; 17)		442	83	91
Mayinger et al [71]	2004	<i>in vivo</i>	31		375–478	69	87
Kamath et al [72]	2008	<i>ex-vivo</i>		23 (13, 10)	325	93.5	100
Bergholt et al [73]	2011	<i>in vivo</i>	81	176	785	98.6	84.7
Boerwinkel et al [74]	2015	<i>in vivo</i>	47 (12; 35)	151 (108; 43)	405	81	58
Ehlen et al [75]	2019	<i>ex-vivo</i>	10	95 (45; 50)	473	87	78
<b>MEAN <math>\pm</math> SD</b>						<b>90 <math>\pm</math> 10</b>	<b>85 <math>\pm</math> 15</b>

<sup>a</sup> Number of patients and tissue areas/biopsies effectively included in each study, i.e. non-counting the ones excluded from analysis due to artefacts or other reasons. In brackets, the number of non-tumour (N-T) and tumour (T) sites.

**Table A2.** List of studies reporting the detection of gastrointestinal tumours by reflectance spectroscopy or imaging.

Paper	Year	Type	Patients <sup>a</sup>	Sites <sup>a</sup> (N-T; T)	Detection (nm)	Sens. (%)	Spec. (%)
Ge et al [63]	1998	<i>in vivo</i>		160 (107; 53)	350–800	85 <sup>b</sup>	85 <sup>b</sup>
Dhar et al [76]	2006	<i>in vivo</i>	45	138	300–800	80	86
Akbari et al [77]	2011	<i>ex-vivo</i>	10	101	1000–2500	91	93
Kiyotoki et al [78]	2013	<i>ex-vivo</i>	14	320 (160; 160)	400–800	76.2	78.8
Evers et al [79]	2013	<i>ex-vivo</i>	24	828 (393; 435)	500–1600	94	94
Kumashiro et al [80]	2016	<i>in vivo</i>	24	135 (95; 40)	450–600	72.5	82.1
Han et al [81]	2016	<i>in vivo</i>	12	21	405–665	97	91
Tanis et al [82]	2016	<i>in vivo</i>	17	484	400–1600	95	92
Keller et al [83]	2018	<i>ex-vivo</i>	32	254 (123; 131)	344–1044	98.4	99.2
Ehlen et al [75]	2019	<i>ex-vivo</i>	10	95 (45; 50)	901–1301	93	68
Baltussen et al [84]	2019	<i>in vivo</i>	32	270	400–1700	90	94
Nogueira et al [85]	2021	<i>ex-vivo</i>	47		350–1919	96.1	95.7
<b>MEAN <math>\pm</math> SD</b>						<b>89 <math>\pm</math> 9</b>	<b>88 <math>\pm</math> 9</b>

<sup>a</sup> Number of patients and tissue areas/biopsies effectively included in each study, i.e. non-counting the ones excluded from analysis due to artefacts or other reasons. In brackets, the number of non-tumour (N-T) and tumour (T) sites.

<sup>b</sup> Values corresponding to the mean predictive accuracy.

**Table A3.** List of studies reporting the detection of gastrointestinal tumours by Raman spectroscopy.

Paper	Year	Type	Patients <sup>a</sup> (N-T; T)	Sites <sup>a</sup> (N-T; T)	Spectra (N-T; T)	$\lambda_{exc}$ (nm)	Sens. (%)	Spec. (%)
Stone et al [65]	2002	<i>ex-vivo</i>	44	89	617 (455; 162)	830	94	93
Kendall et al [66]	2003	<i>ex-vivo</i>	44	87 (53; 34)	1125	830	94	93
Teh et al [67]	2008	<i>ex-vivo</i>	53	73 (55; 18)	222 (143; 79)	785	90.2	95.7
Huang et al [86]	2010	<i>in vivo</i>	67	238 (121; 117)	1063	785	94.0	93.4
Teh et al [87]	2010	<i>ex-vivo</i>	62	100 (70; 30)		785	80	91
Bergholt et al [88]	2011	<i>in vivo</i>	67 (63; 61)	238 (121; 117)	1063 (934; 129)	785	94.6	94.6
Bergholt et al [73]	2011	<i>in vivo</i>	81	176	1238 (1098; 140)	785	92.9	89.3
Kawabata et al [89]	2011	<i>ex-vivo</i>	10		213 (132; 81)	1040	73	73
Duraipandian et al [90]	2012	<i>in vivo</i>	305		2748 (2465; 283)	785	80.5	86.2
Bergholt et al [91]	2013	<i>in vivo</i>	83		1277 (1013; 264)	785	84.9	95.6
Jin and Mao [92]	2014	<i>ex-vivo</i>	105 (72; 33)			NIR	100	97.4
Wang et al [93]	2016	<i>in vivo</i>	191 (178; 13)	441 (407; 34)	5792 (5315; 477)	785	82.4	94.3
Petersen et al [94]	2017	<i>ex-vivo</i>	69 (56, 13)	123 (101, 22)	269 (204, 65)	785	79	83
<b>MEAN <math>\pm</math> SD</b>							<b>88 <math>\pm</math> 8</b>	<b>91 <math>\pm</math> 7</b>

<sup>a</sup> Number of patients and tissue areas/biopsies effectively included in each study, i.e. non-counting the ones excluded from analysis due to artefacts or other reasons. In brackets, the number of non-tumour (N-T) and tumour (T) sites.

**Table A4.** List of studies reporting the detection of gastrointestinal cancer by nonlinear techniques.

Author	Tissue	Signal collected	Type	$\lambda_{exc}$ (nm)	Year
Zheng et al [99]	Oral cheek pouch	TPEF/SHG	<i>in-vivo</i>	745	2011
Orzekowsky-Schroeder et al [100]	Small intestine	TPEF**	<i>in-vivo</i>	730–910	2011
Cicchi et al [101]	Colon mucosa	TPEF	<i>ex-vivo</i>	740	2013
Makino et al [102]	Oesophagus, stomach, duodenum, ileum, and colon	SHG/TPEF	<i>ex-vivo</i>	780	2013
Chen et al [103]	Oesophagus, gastroesophageal junction (GEJ), and gastric cardia*	TPEF**/SHG	<i>ex-vivo</i>	735/800	2014
Stanciu et al [104]	Liver	TPEF/SHG	<i>ex-vivo</i>	900	2014
Li et al [105]	Colorectal	TPEF/SHG	<i>ex-vivo</i>	810	2014
Schueth et al [106]	Bladder	TPEF/SHG	<i>ex-vivo</i>	800	2014
Yan et al [107]	Rectal	TPEF/SHG	<i>ex-vivo</i>	800	2014
Klinger et al [51]	Murine intestinal mucosa	TPEF**	<i>in-vivo</i>	730/800 vs 800 (10fs)	2015
Zhou et al [108]	Gastric muscularis propria*	TPEF/SHG	<i>ex-vivo</i>	810	2016
Skala et al [109]	Hamster cheek pouch	SHG/ TPEF	<i>ex-vivo</i>	780	2017
Matsui et al [110]	Colorectal*	TPEF**/SHG	<i>ex-vivo</i>	730/820/900	2017
Sarri et al [111]	Colon pancreas*	SRS/SHG/CARS/ TPEF	<i>ex-vivo</i>	1030 + 790-800	2019
Li et al [112]	Gastric	TPEF/SHG	<i>ex-vivo</i>	810	2019
Chen et al [43]	Oesophagus*	TPEF/SHG	<i>ex-vivo</i>	810	2020
Shen et al [113]	Pancreas and liver	THG/FLIM/3PEF/ TPEF/SHG	<i>in-vivo</i>	1140	2020
Zhang et al [114]	Laryngeal squamous	3PFE/SHG/ THG	<i>ex-vivo</i>	1050 (40fs)	2021

\*Studies on human tissue.

\*\* Endogenous Two-Photon Excited Fluorescence Imaging.

**Table A5.** List of studies reporting the detection of bladder tumours by fluorescence spectroscopy.

Paper	Year	Type	Patients <sup>a</sup>	Sites <sup>a</sup> (N-T; T)	$\lambda_{exc}$ (nm)	Sens. (%)	Spec. (%)
D'Hallewin et al [115]	1994	<i>in vivo</i>	>10		365		
Koenig et al [116]	1996	<i>in vivo</i>	53	114 (29; 85)	337	97	98
Anidjar et al [120]	1996	<i>ex-vivo</i>		21 (9; 12)	308	100	100
Zaak et al [117]	2002	<i>in vivo</i>	43	114 (21; 93)	308	95	77
Zheng et al [121]	2003	<i>ex-vivo</i>	25	52 (14; 38)	280	97	93
					330	95	92
Aboumarzouk et al [118]	2015	<i>in vivo</i>	21	63 (37; 30)	405		
Kriegmair et al [119]	2018	<i>in vivo</i>	25	56 (26; 30)	440	96.7	53.8
Baria et al [60]	2019	<i>ex-vivo</i>	32	50 (20; 30)	378	100	100
					445	95	100
Morselli et al [61]	2021	<i>ex-vivo</i>	114	169 (40; 129)	378	79	80
					445	70	89
<b>MEAN <math>\pm</math> SD</b>						<b>92 <math>\pm</math> 10</b>	<b>88 <math>\pm</math> 15</b>

<sup>a</sup> Number of patients and tissue areas/biopsies effectively included in each study, i.e. non-counting the ones excluded from analysis due to artefacts or other reasons. In brackets, the number of non-tumour (N-T) and tumour (T) sites.**Table A6.** List of studies reporting the detection of bladder tumours by reflectance spectroscopy or imaging.

Paper	Year	Type	Patients <sup>a</sup> (N-T; T)	Sites <sup>a</sup> (N-T; T)	Detection (nm)	Sens. (%)	Spec. (%)
Mourant et al [122]	1995	<i>in vivo</i>	10	50 (30; 20)	250–800	100	97
Koenig et al [123]	1998	<i>in vivo</i>	14	26 (17; 9)	450–700	91	60
Herr and Donat [126]	2008	<i>in vivo</i>	427		415 $\pm$ 30	100	82
					540 $\pm$ 30		
Tatsugami [127]	2010	<i>in vivo</i>	104	313	415 $\pm$ 30	92.7	70.9
					540 $\pm$ 30		
Chen et al [128]	2013	<i>in vivo</i>	143	(NA; 285)	415 $\pm$ 30	79	79
					540 $\pm$ 30		
Ye et al [129]	2015	<i>in vivo</i>	103 (16; 87)	300	415 $\pm$ 30	98.8	60.9
					540 $\pm$ 30		
Slaton et al [124]	2016	<i>in vivo</i> <sup>b</sup>	6 (2; 4)	108 (27; 81)	520–920		
Baria et al [60]	2019	<i>ex-vivo</i>	32	50 (20; 30)	440–710	90	83
Morselli et al [61]	2021	<i>ex-vivo</i>	114	169 (40; 129)	440–710	66	65
<b>MEAN <math>\pm</math> SD</b>						<b>90 <math>\pm</math> 12</b>	<b>75 <math>\pm</math> 13</b>

<sup>a</sup> Number of patients and tissue areas/biopsies effectively included in each study, i.e. non-counting the ones excluded from analysis due to artefacts or other reasons. In brackets, the number of non-tumour (N-T) and tumour (T) sites.<sup>b</sup> Study conducted on animal model.

**Table A7.** List of studies reporting the detection of bladder tumours by Raman spectroscopy.

Paper	Year	Type	Patients <sup>a</sup>	Sites <sup>a</sup> (N-T; T)	Spectra (N-T; T)	$\lambda_{\text{exc}}$ (nm)	Sens. (%)	Spec. (%)
Stone <i>et al</i> [65]	2002	<i>ex-vivo</i>	12	12	196 (15; 181)	830	99	93
Crow <i>et al</i> [130]	2004	<i>ex-vivo</i>	72	75	1525	830	97	95
Crow <i>et al</i> [131]	2005	<i>ex-vivo</i>		29	220	785	79	89
de Jong <i>et al</i> [137]	2006	<i>ex-vivo</i>	15	90 (37; 53)		845	94	92
Draga <i>et al</i> [132]	2010	<i>in vivo</i>	32		63 (28; 35)	785	85	79
Barman <i>et al</i> [133]	2012	<i>ex-vivo</i>	14	28 (14; 14)	140 (70; 70)	785	85.7	100
Wang <i>et al</i> [233]	2012	<i>ex-vivo</i>				632.8	87.7	87.5
Chen <i>et al</i> [136]	2018	<i>ex-vivo</i>	10	32	262 (78; 184)	785	95.1	88.5
Baria <i>et al</i> [60]	2019	<i>ex-vivo</i>	32	50 (20; 30)	50 (20; 30)	785	95	87
Cordero <i>et al</i> [134]	2019	<i>ex-vivo</i>	21	48		785	92	93
Placzek <i>et al</i> [135]	2020	<i>ex-vivo</i>	44	116 (66; 50)	~100 000	785	95	88
Morselli <i>et al</i> [61]	2021	<i>ex-vivo</i>	114	169 (40; 129)	169 (40; 129)	785	77	72
<b>MEAN <math>\pm</math> SD</b>							<b>90 <math>\pm</math> 7</b>	<b>89 <math>\pm</math> 7</b>

<sup>a</sup> Number of patients and tissue areas/biopsies effectively included in each study, i.e. non-counting the ones excluded from analysis due to artefacts or other reasons. In brackets, the number of non-tumour (N-T) and tumour (T) sites.

**Table A8.** List of studies reporting the discrimination between LG and HG bladder tumours by Raman spectroscopy.

Paper	Year	Type	$\lambda_{\text{exc}}$ (nm)	Sens. (%)	Spec. (%)
Crow <i>et al</i> [130]	2004	<i>ex-vivo</i>	830	98 <sup>a</sup>	93 <sup>a</sup>
Bovenkamp <i>et al</i> [234]	2018	<i>ex-vivo</i>	785	99	87
Chen <i>et al</i> [136]	2018	<i>ex-vivo</i>	785	97.5 <sup>a</sup>	96.4 <sup>a</sup>
Baria <i>et al</i> [60]	2019	<i>ex-vivo</i>	785	90	90
Cordero <i>et al</i> [134]	2019	<i>ex-vivo</i>	785	85	83
Placzek <i>et al</i> [135]	2020	<i>ex-vivo</i>	785	81	68
Morselli <i>et al</i> [61]	2021	<i>ex-vivo</i>	785	73	65
<b>MEAN <math>\pm</math> SD</b>				<b>89 <math>\pm</math> 10</b>	<b>83 <math>\pm</math> 12</b>

<sup>a</sup> These values represent sensitivity and specificity in discriminating HG spectra from both non-tumour and LG spectra.

**Table A9.** List of studies reporting the detection of bladder tumours by non-linear techniques.

Paper	Tissue	Technique	Year	$\lambda_{\text{exc}}$ (nm)	Type
Mukherjee <i>et al</i> [138]	Bladder	SHG/TPEF	2009	785	<i>ex-vivo</i>
Cicchi <i>et al</i> [139]	Bladder	SHG/TPEF/FLIM	2010	790	<i>ex-vivo</i>
Jain <i>et al</i> [140]	Bladder	SHG/TPEF	2012	785	<i>ex-vivo</i>
Katz <i>et al</i> [141]	Bladder- prostate	SHG/TPEF	2014	785	<i>ex-vivo</i>
Jain <i>et al</i> [143]	Bladder	SHG/TPEF	2015	785	<i>ex-vivo</i>
Marchetti <i>et al</i> [142]	Bladder	ALL	2019	1040 + 785	<i>ex-vivo</i>

**Table A10.** List of studies reporting multimodal techniques using an endoscope.

Author	Tissue	Non-linear effect reported	Excitation wavelength (nm)	Year
Zhao <i>et al</i> [153]	Human Trabecular (stained)	TPEF	800	2010
Rivera <i>et al</i> [154]	Mouse tail tendon Mouse colon Mouse lung	TPEF/SHG	800	2011
Brown <i>et al</i> [155]	Rat kidney ( <i>ex-vivo</i> ) Rat colon ( <i>in-vivo</i> )	TPEF/SHG	800	2012
Liang <i>et al</i> [156]	Rat kidney renal cortex Rat inner colon wall Rat liver	TPEF/SHG	800	2012
Huland <i>et al</i> [157]	A431 cancer cells (stained)	TPEF/OCT	1550	2012
Xi <i>et al</i> [158]	Mouse liver ( <i>ex-vivo</i> ) Mouse small intestine ( <i>in-vivo</i> )	TPEF/SHG	810	2017
Lombardini <i>et al</i> [160]	Human colon fatty tissues	SHG/CARS	800/1040	2018
Dilipkumar <i>et al</i> [161]	Murine colon mucosa <i>in vivo</i>	TPEF/SHG	780	2019

**Table A11.** List of studies reporting improvements in the microendoscope.

Author	Non-linear effect reported	Excitation wavelength (nm)	Year	Improvement provided
Liang et al [156]	TPEF	810	2012	Increased illumination uniformity and reduced photodamage
Ouzounov et al [162]	TPEF	800	2013	Add optical zoom capability
Lefort et al [163]	TPEF	800	2014	Improving and characterizing of a commercial double-clad fiber
Ducourthial et al [164]	TPEF/SHG	810	2015	Improving acquisition time
Hamzeh et al [165]	TPEF	750–810	2015	Optimization and characterization of GRIN lens
Kim et al [166]	TPEF		2016	Incorporating a Polarization Maintaining
Pshenay-Severin et al [167]	CARS, TPEF, SHG	795/1030	2021	Laser transmission and signal collection for CARS, SHG, and TPEF

## ORCID iDs

G Castro-Olvera  <https://orcid.org/0000-0001-9843-3581>

A Koviakov  <https://orcid.org/0000-0002-2668-2367>

R Gumenyuk  <https://orcid.org/0000-0002-0679-9189>

## References

- [1] Sung H, Ferlay J, Siegel R L, Laversanne M, Soerjomataram I, Jemal A and Bray F 2021 Global cancer statistics 2020: GLOBOCAN estimates of incidence and mortality worldwide for 36 cancers in 185 countries *Cancer J. Clinicians* **71** 209–49
- [2] Ferlay J, Steliarova-Foucher E, Lortet-Tieulent J, Rosso S, Coebergh J W W, Comber H, Forman D and Bray F 2013 Cancer incidence and mortality patterns in Europe: estimates for 40 countries in 2012 *Eur. J. Cancer* **49** 1374–403
- [3] Ferlay J and Laversanne M 2020 *Global Cancer Observatory: Cancer Tomorrow* (International Agency for Research on Cancer)
- [4] Cumberbatch M G K, Cox A, Teare D and Catto J W F 2015 Contemporary occupational carcinogen exposure and bladder cancer *JAMA Oncol.* **1** 1282
- [5] Antoni S, Ferlay J, Soerjomataram I, Znaor A, Jemal A and Bray F 2017 Bladder cancer incidence and mortality: a global overview and recent trends *Eur. Urol.* **71** 96–108
- [6] Araghi M, Soerjomataram I, Jenkins M, Brierley J, Morris E, Bray F and Arnold M 2019 Global trends in colorectal cancer mortality: projections to the year 2035 *Int. J. Cancer* **144** 2992–3000
- [7] Fernando H, Thota S S, Burt G, Waterfall N and Husain I 2007 Importance of red patches diagnosed in cystoscopy for haematuria and lower urinary tract symptoms *Postgraduate Med. J.* **83** 62–63
- [8] Beg S, Wilson A and Ragnunath K 2016 The use of optical imaging techniques in the gastrointestinal tract *Frontline Gastroenterol.* **7** 207–15
- [9] Oka K et al 2021 Clinical features of false-negative early gastric cancers: a retrospective study of endoscopic submucosal dissection cases *Gastroenterol. Res. Pract.* **2021** 1–9
- [10] Fukuhara H, Yamamoto S, Karashima T and Inoue K 2021 Photodynamic diagnosis and therapy for urothelial carcinoma and prostate cancer: new imaging technology and therapy *Int. J. Clin. Oncol.* **26** 18–25
- [11] Wu J, Wang Y-C, Dai B, Ye D-W and Zhu Y-P 2019 Optical biopsy of bladder cancer using confocal laser endomicroscopy *Int. Urol. Nephrol.* **51** 1473–9
- [12] Baria E, Morselli S, Anand S, Fantechi R, Nesi G, Gacci M, Carini M, Serni S, Cicchi R and Pavone F S 2019 Label-free grading and staging of urothelial carcinoma through multimodal fibre-probe spectroscopy *J. Biophoton.* **12** e201900087
- [13] Morselli S, Baria E, Cicchi R, Liaci A, Sebastianelli A, Nesi G, Serni S, Pavone F S and Gacci M 2021 The feasibility of multimodal fiber optic spectroscopy analysis in bladder cancer detection, grading, and staging *Urol. J.* **88** 306–14
- [14] Kurilchik S et al 2020 Advanced multimodal laser imaging tool for urothelial carcinoma diagnosis (AMPLITUDE) *J. Phys. Photon.* **2** 021001
- [15] Castro-Olvera G, Serni S, Liaci A, Morselli S, Gacci M, Nicoletti R and Loza-Alvarez P 2021 Multimodal SWIR laser imaging for assessment and detection of urothelial carcinomas *Short-Wavelength Infrared Windows for Biomedical Applications* ed L A Sordillo and P P Sordillo (SPIE)
- [16] Yamamoto S, Fukuhara H, Karashima T and Inoue K 2020 Real-world experience with 5-aminolevulinic acid for the photodynamic diagnosis of bladder cancer: diagnostic accuracy and safety *Photodiagn. Photodyn. Ther.* **32** 101999
- [17] Zheng C, Lv Y, Zhong Q, Wang R and Jiang Q 2012 *Narrow Band Imaging Diagnosis of Bladder Cancer: Systematic Review and Meta-analysis* (BJU International)
- [18] Loidl W, Schmidbauer J, Susani M and Marberger M 2005 Flexible cystoscopy assisted by hexaminolevulinic acid induced fluorescence: a new approach for bladder cancer detection and surveillance? *Eur. Urol.* **47** 323–6
- [19] Bryan R T, Billingham L J and Wallace D M A 2008 Narrow-band imaging flexible cystoscopy in the detection of recurrent urothelial cancer of the bladder *BJU Int.* **101** 702–6
- [20] Kamphuis G M, de Bruin D M, Brandt M J, Knoll T, Conort P, Lapini A, Dominguez-Escrig J L and de la Rosette J J M C H 2016 Comparing image perception of bladder tumors in four different storz professional image enhancement system modalities using the iSPIES app *J. Endourol.* **30** 602–8
- [21] Marti A, Lange N, Van Den Bergh H, Sedmera D, Jichlinski P and Kucera P 1999 Optimisation of the formation and distribution of protoporphyrin IX in the urothelium: an in vitro approach *J. Urol.* **162** 546–52

- [22] Holth L, Eder I E, Klocker H, Hobisch A, Bartsch G and Stenzl A 2001 Photodynamic diagnosis with 5-aminolevulinic acid in the treatment of secondary urethral tumors: first *in vitro* and *in vivo* results *Eur. Urol.* **39** 178–82
- [23] Chauhan S S et al 2014 Confocal laser endomicroscopy *Gastrointest. Endosc.* **80** 928–38
- [24] Neumann H, Kiesslich R, Wallace M B and Neurath M F 2010 Confocal laser endomicroscopy: technical advances and clinical applications *Gastroenterology* **139** 388–92.e2
- [25] Marien A, Rock A, Maadarani K E, Francois C, Gosset P, Mauroy B and Bonnal J-L 2017 Urothelial tumors and dual-band imaging: a new concept in confocal laser endomicroscopy *J. Endourol.* **31** 538–44
- [26] Wiesner C, Jäger W, Salzer A, Biesterfeld S, Kiesslich R, Hampel C, Thüroff J W and Goetz M 2011 Confocal laser endomicroscopy for the diagnosis of urothelial bladder neoplasia: a technology of the future? *BJU Int.* **107** 399–403
- [27] Bui D, Mach K E, Zlatev D V, Rouse R V, Leppert J T and Liao J C 2015 A pilot study of *in vivo* confocal laser endomicroscopy of upper tract urothelial carcinoma *J. Endourol.* **29** 1418–23
- [28] Beji S, Wrist Lam G, Østergren P B, Toxvaerd A, Sønksen J and Fode M 2021 Diagnostic value of probe-based confocal laser endomicroscopy versus conventional endoscopic biopsies of non-muscle invasive bladder tumors: a pilot study *Scand. J. Urol.* **55** 36–40
- [29] Fugazza A, Gaiani F, Carra M C, Brunetti F, Lévy M, Sobhani I, Azoulay D, Catena F, de'Angelis G L and de'Angelis N 2016 Confocal laser endomicroscopy in gastrointestinal and pancreatobiliary diseases: a systematic review and meta-analysis *Biomed. Res. Int.* **2016** 1–31
- [30] Zonios G, Bykowski J and Kollias N 2001 Skin melanin, hemoglobin, and light scattering properties can be quantitatively assessed *in vivo* using diffuse reflectance spectroscopy *J. Invest. Dermatol.* **117** 1452–7
- [31] Filip M 2011 Autofluorescence imaging and magnification endoscopy *World J. Gastroenterol.* **17** 9
- [32] Song L M W K et al 2011 Autofluorescence imaging *Gastrointest. Endosc.* **73** 647–50
- [33] Aihara H, Tajiri H and Suzuki T 2012 Application of autofluorescence endoscopy for colorectal cancer screening: rationale and an update *Gastroenterol. Res. Pract.* **2012** 1–5
- [34] Tajiri H 2007 Autofluorescence endoscopy for the gastrointestinal tract *Proc. Japan Acad. B* **83** 248–55
- [35] Lakowicz J R 2006 *Principles of Fluorescence Spectroscopy* 3rd edn (Springer) (<https://doi.org/10.1007/978-0-387-46312-4>)
- [36] Wagnieres G A, Star W M and Wilson B C 1998 *In vivo* fluorescence spectroscopy and imaging for oncological applications *Photochem. Photobiol.* **68** 603–32
- [37] Croce A C and Bottiroli G 2014 Autofluorescence spectroscopy and imaging: a tool for biomedical research and diagnosis *Eur. J. Histochem.* **58** 320–37
- [38] Bachmann L, Zezell D M, Ribeiro A D C, Gomes L and Ito A S 2006 Fluorescence spectroscopy of biological tissues—A review *Appl. Spectrosc. Rev.* **41** 575–90
- [39] Moriichi K, Fujiya M and Okumura T 2016 The efficacy of autofluorescence imaging in the diagnosis of colorectal diseases *Clin. J. Gastroenterol.* **9** 175–83
- [40] Movasaghi Z, Rehman S and Rehman I U 2007 Raman spectroscopy of biological tissues *Appl. Spectrosc. Rev.* **42** 493–541
- [41] Choo-Smith L-P, Edwards H G M, Endtz H P, Kros J M, Heule F, Barr H, Robinson J S, Bruining H A and Puppels G J 2002 Medical applications of Raman spectroscopy: from proof of principle to clinical implementation *Biopolymers* **67** 1–9
- [42] Alizadeh M, Merino D, Lombardo G, Lombardo M, Mencucci R, Ghotbi M and Loza-Alvarez P 2019 Identifying crossing collagen fibers in human corneal tissues using pSHG images *Biomed. Opt. Express* **10** 3875
- [43] Chen W-C et al 2020 Label-free characterization of collagen fibers in cancerous esophagus tissues using ratiometric nonlinear optical microscopy *Exp. Biol. Med.* **245** 1213–21
- [44] Lombardo M, Merino D, Loza-Alvarez P and Lombardo G 2015 Translational label-free nonlinear imaging biomarkers to classify the human corneal microstructure *Biomed. Opt. Express* **6** 2803
- [45] Psilodimitrakopoulos S, Artigas D, Soria G, Amat-Roldan I, Planas A M and Loza-Alvarez P 2009 Quantitative discrimination between endogenous SHG sources in mammalian tissue, based on their polarization response *Opt. Express* **17** 10168
- [46] Psilodimitrakopoulos S, Petegnief V, Soria G, Amat-Roldan I, Artigas D, Planas A M and Loza-Alvarez P 2009 Estimation of the effective orientation of the SHG source in primary cortical neurons *Opt. Express* **17** 14418
- [47] Psilodimitrakopoulos S, Loza-Alvarez P and Artigas D 2014 Fast monitoring of *in-vivo* conformational changes in myosin using single scan polarization-SHG microscopy *Biomed. Opt. Express* **5** 4362
- [48] Amat-Roldan I, Psilodimitrakopoulos S, Loza-Alvarez P and Artigas D 2010 Fast image analysis in polarization SHG microscopy *Opt. Express* **18** 17209
- [49] Psilodimitrakopoulos S, Amat-Roldan I, Loza-Alvarez P and Artigas D 2012 Effect of molecular organization on the image histograms of polarization SHG microscopy *Biomed. Opt. Express* **3** 2681
- [50] Aviles-Espinosa R 2010 Third-harmonic generation for the study of 'Caenorhabditis elegans' embryogenesis *J. Biomed. Opt.* **15** 046020
- [51] Klinger A, Krapf L, Orzekowsky-Schroeder R, Koop N, Vogel A and Hüttmann G 2015 Intravital autofluorescence 2-photon microscopy of murine intestinal mucosa with ultra-broadband femtosecond laser pulse excitation: image quality, photodamage, and inflammation *J. Biomed. Opt.* **20** 1
- [52] Chaumel J, Marsal M, Gómez-Sánchez A, Blumer M, Gualda E J, de Juan A, Loza-Alvarez P and Dean M N 2021 Autofluorescence of stingray skeletal cartilage: hyperspectral imaging as a tool for histological characterization *Discov. Mater.* **1** 16
- [53] Oheim M, Beaurepaire E, Chaigneau E, Mertz J and Charpak S 2001 Two-photon microscopy in brain tissue: parameters influencing the imaging depth *J. Neurosci. Methods* **111** 29–37
- [54] Resan B, Aviles-Espinosa R, Kurmulis S, Licea-Rodríguez J, Brunner F, Rohrbacher A, Artigas D, Loza-Alvarez P and Weingarten K J 2014 Two-photon fluorescence imaging with 30 fs laser system tunable around 1  $\mu\text{m}$  *Opt. Express* **22** 16456–61
- [55] De Meulenaere E et al 2012 Molecular engineering of chromophores for combined second-harmonic and two-photon fluorescence in cellular imaging *Chem. Sci.* **3** 984
- [56] Aviles-Espinosa R et al 2011 Compact ultrafast semiconductor disk laser: targeting GFP based nonlinear applications in living organisms *Biomed. Opt. Express* **2** 739
- [57] Wang T and Xu C 2020 Three-photon neuronal imaging in deep mouse brain *Optica* **7** 947–60
- [58] Streich L, Boffi J C, Wang L, Alhalaseh K, Barbieri M, Rehm R, Deivasigamani S, Gross C T, Agarwal A and Prevedel R 2021 High-resolution structural and functional deep brain imaging using adaptive optics three-photon microscopy *Nat. Methods* **18** 1253–8
- [59] Kapadia C R, Cutruzzola F W, O'Brien K M, Stetz M L, Enriquez R and Deckelbaum L I 1990 Laser-induced fluorescence spectroscopy of human colonic mucosa *Gastroenterology* **99** 150–7

- [60] Marchesini R, Brambilla M, Pignoli E, Bottiroli G, Croce A C, Dal Fante M, Spinelli P and Di Palma S 1992 Light-induced fluorescence spectroscopy of adenomas, adenocarcinomas and non-neoplastic mucosa in human colon I. In vitro measurements *J. Photochem. Photobiol. B* **14** 219–30
- [61] Chwirot B W, Chwirot S, Jedrzejczyk W, Jackowski M, Raczyńska A M, Winczakiewicz J and Dobber J 1997 Ultraviolet laser-induced fluorescence of human stomach tissues: detection of cancer tissues by imaging techniques *Lasers Surg. Med.* **21** 149–58
- [62] Cothren R M et al 1990 Gastrointestinal tissue diagnosis by laser-induced fluorescence spectroscopy at endoscopy *Gastrointest. Endosc.* **36** 105–11
- [63] Ge Z, Schomacker K T and Nishioka N S 1998 Identification of colonic dysplasia and neoplasia by diffuse reflectance spectroscopy and pattern recognition techniques *Appl. Spectrosc.* **52** 833–9
- [64] Mourant J R 1996 Elastic scattering spectroscopy as a diagnostic tool for differentiating pathologies in the gastrointestinal tract: preliminary testing *J. Biomed. Opt.* **1** 192
- [65] Stone N, Kendall C, Shepherd N, Crow P and Barr H 2002 Near-infrared Raman spectroscopy for the classification of epithelial pre-cancers and cancers *J. Raman Spectrosc.* **33** 564–73
- [66] Kendall C, Stone N, Shepherd N, Geboes K, Warren B, Bennett R and Barr H 2003 Raman spectroscopy, a potential tool for the objective identification and classification of neoplasia in Barrett's oesophagus *J. Pathol.* **200** 602–9
- [67] Teh S K, Zheng W, Ho K Y, Teh M, Yeoh K G and Huang Z 2008 Diagnosis of gastric cancer using near-infrared Raman spectroscopy and classification and regression tree techniques *J. Biomed. Opt.* **13** 034013
- [68] Kobayashi M, Tajiri H, Seike E, Shitaya M, Tounou S, Mine M and Oba K 2001 Detection of early gastric cancer by a real-time autofluorescence imaging system *Cancer Lett.* **165** 155–9
- [69] Mayinger B, Horner P, Jordan M, Gerlach C, Horbach T, Hohenberger W and Hahn E G 2001 Light-induced autofluorescence spectroscopy for the endoscopic detection of esophageal cancer *Gastrointest. Endosc.* **54** 195–201
- [70] Xiao S D, Ge Z Z, Zhong L and Luo H Y 2002 Diagnosis of gastric cancer by using autofluorescence spectroscopy *Chin. J. Digestive Dis.* **3** 99–102
- [71] Mayinger B, Jordan M, Horbach T, Horner P, Gerlach C, Mueller S, Hohenberger W and Hahn E G 2004 Evaluation of *in vivo* endoscopic autofluorescence spectroscopy in gastric cancer *Gastrointest. Endosc.* **59** 191–8
- [72] Kamath S D, D'souza C S, Mathew S, George S D, Santhosh C and Mahato K K 2008 A pilot study on colonic mucosal tissues by fluorescence spectroscopy technique: discrimination by principal component analysis (PCA) and artificial neural network (ANN) analysis *J. Chemometr.* **22** 408–16
- [73] Bergholt M S, Zheng W, Lin K, Ho K Y, Teh M, Yeoh K G, So J B Y and Huang Z 2011 Combining near-infrared-excited autofluorescence and Raman spectroscopy improves *in vivo* diagnosis of gastric cancer *Biosens. Bioelectron.* **26** 4104–10
- [74] Boerwinkel D F, Holz J A, Hawkins D M, Curvers W L, Aalders M C, Weusten B L, Visser M, Meijer S L and Bergman J J 2015 Fluorescence spectroscopy incorporated in an optical biopsy system for the detection of early neoplasia in Barrett's esophagus: optical biopsy system *Dis. Esophagus* **28** 345–51
- [75] Ehlen L et al 2019 Synergy of fluorescence and near-infrared spectroscopy in detection of colorectal cancer *J. Surg. Res.* **242** 349–56
- [76] Dhar A, Johnson K S, Novelli M R, Bown S G, Bigio I J, Lovat L B and Bloom S L 2006 Elastic scattering spectroscopy for the diagnosis of colonic lesions: initial results of a novel optical biopsy technique *Gastrointest. Endosc.* **63** 257–61
- [77] Akbari H, Uto K, Kosugi Y, Kojima K and Tanaka N 2011 Cancer detection using infrared hyperspectral imaging *Cancer Sci.* **102** 852–7
- [78] Kiyotoki S et al 2013 New method for detection of gastric cancer by hyperspectral imaging: a pilot study *J. Biomed. Opt.* **18** 026010
- [79] Evers D J, Nachabé R, Hompes D, van Coevorden F, Lucassen G W, Hendriks B H W, van Velthuysen M-L F, Wesseling J and Ruers T J M 2013 Optical sensing for tumor detection in the liver *Eur. J. Surg. Oncol.* **39** 68–75
- [80] Kumashiro R, Konishi K, Chiba T, Akahoshi T, Nakamura S, Murata M, Tomikawa M, Matsumoto T, Maehara Y and Hashizume M 2016 Integrated endoscopic system based on optical imaging and hyperspectral data analysis for colorectal cancer detection *Anticancer Res.* **36** 3925
- [81] Han Z, Zhang A, Wang X, Sun Z, Wang M D and Xie T 2016 *In vivo* use of hyperspectral imaging to develop a noncontact endoscopic diagnosis support system for malignant colorectal tumors *J. Biomed. Opt.* **21** 016001
- [82] Tanis E, Evers D J, Spliethoff J W, Pully V V, Kuhlmann K, van Coevorden F, Hendriks B H W, Sanders J, Prevoo W and Ruers T J M 2016 *In vivo* tumor identification of colorectal liver metastases with diffuse reflectance and fluorescence spectroscopy *Lasers Surg. Med.* **48** 820–7
- [83] Keller A, Bialecki P, Wilhelm T J and Vetter M K 2018 Diffuse reflectance spectroscopy of human liver tumor specimens—towards a tissue differentiating optical biopsy needle using light emitting diodes *Biomed. Opt. Express* **9** 1069
- [84] Baltussen E J M, Brouwer de Koning S G, Sanders J, Aalbers A G J, Kok N F M, Beets G L, Hendriks B H W, Sterenborg H J C M, Kuhlmann K F D and Ruers T J M 2019 Tissue diagnosis during colorectal cancer surgery using optical sensing: an *in vivo* study *J. Transl. Med.* **17** 333
- [85] Nogueira M S, Maryam S, Amisshah M, Lu H, Lynch N, Killeen S, O'Riordain M and Andersson-Engels S 2021 Evaluation of wavelength ranges and tissue depth probed by diffuse reflectance spectroscopy for colorectal cancer detection *Sci. Rep.* **11** 798
- [86] Huang Z, Teh S K, Zheng W, Lin K, Ho K Y, Teh M and Yeoh K G 2010 *In vivo* detection of epithelial neoplasia in the stomach using image-guided Raman endoscopy *Biosens. Bioelectron.* **26** 383–9
- [87] Teh S K, Zheng W, Ho K Y, Teh M, Yeoh K G and Huang Z 2010 Near-infrared Raman spectroscopy for early diagnosis and typing of adenocarcinoma in the stomach *Br. J. Surg.* **97** 550–7
- [88] Bergholt M S, Zheng W, Lin K, Ho K Y, Teh M, Yeoh K G, Yan So J B and Huang Z 2011 *In vivo* diagnosis of gastric cancer using Raman endoscopy and ant colony optimization techniques *Int. J. Cancer* **128** 2673–80
- [89] Kawabata T et al 2011 Near-infrared multichannel raman spectroscopy with a 1064 nm excitation wavelength for *ex vivo* diagnosis of gastric cancer *J. Surg. Res.* **169** e137–43
- [90] Duraipandian S, Sylvest Bergholt M, Zheng W, Yu Ho K, Teh M, Guan Yeoh K, Bok Yan So J, Shabbir A and Huang Z 2012 Real-time Raman spectroscopy for *in vivo*, online gastric cancer diagnosis during clinical endoscopic examination *J. Biomed. Opt.* **17** 081418
- [91] Bergholt M S, Zheng W, Ho K Y, Teh M, Yeoh K G, So J B Y, Shabbir A and Huang Z 2013 Fiber-optic Raman spectroscopy probes gastric carcinogenesis *in vivo* at endoscopy *J. Biophoton.* **6** 49–59
- [92] Jin S and Mao H 2014 Near-infrared Raman spectroscopy for diagnosis of gastric cancer *Nan fang yi ke da xue xue bao = J. South. Med. Univ.* **34** 391–5

- [93] Wang J, Lin K, Zheng W, Ho K Y, Teh M, Yeoh K G and Huang Z 2016 Fiber-optic Raman spectroscopy for *in vivo* diagnosis of gastric dysplasia *Faraday Discuss.* **187** 377–92
- [94] Petersen D et al 2017 Raman fiber-optical method for colon cancer detection: cross-validation and outlier identification approach *Spectrochim. Acta A* **181** 270–5
- [95] Ell C 2003 Improving endoscopic resolution and sampling: fluorescence techniques *Gut* **52** 30iv–33
- [96] Angelova L, Borisova E, Zhelyazkova A, Keremedchiev M, Vladimirov B and Avramov L 2013 Fluorescence spectroscopy of gastrointestinal tumors: *in vitro* studies and *in vivo* clinical applications *Proc. SPIE* **9032** 903209
- [97] Liu L, Lin L, Li W, Yang C, Huang Z, Xie S and Li B 2013 Characterizing autofluorescence generated from endogenous porphyrins in cancerous tissue of human colon: case studies *Proc. SPIE* **8577** 857703
- [98] Teh S K, Zheng W, Ho K Y, Teh M, Yeoh K G and Huang Z 2008 Diagnostic potential of near-infrared Raman spectroscopy in the stomach: differentiating dysplasia from normal tissue *Br. J. Cancer* **98** 457–65
- [99] Zheng W, Li D, Li S, Zeng Y, Yang Y and Qu J Y 2011 Diagnostic value of nonlinear optical signals from collagen matrix in the detection of epithelial precancer *Opt. Lett.* **36** 3620
- [100] Orzekowsky-Schroeder R, Klinger A, Martensen B, Blessenohl M, Gebert A, Vogel A and Hüttmann G 2011 *In vivo* spectral imaging of different cell types in the small intestine by two-photon excited autofluorescence *J. Biomed. Opt.* **16** 116025
- [101] Cicchi R, Sturiale A, Nesi G, Kapsokalyvas D, Alemanno G, Tonelli F and Pavone F S 2013 Multiphoton morpho-functional imaging of healthy colon mucosa, adenomatous polyp and adenocarcinoma *Biomed. Opt. Express* **4** 1204
- [102] Makino T et al 2012 Multiphoton tomographic imaging: a potential optical biopsy tool for detecting gastrointestinal inflammation and neoplasia *Cancer Prev. Res.* **5** 1280–90
- [103] Chen J, Wong S, Nathanson M H, Chen J and Jain D 2014 Evaluation of barrett esophagus by multiphoton microscopy *Arch. Pathol. Lab. Med.* **138** 204–12
- [104] Stanciu S G, Xu S, Peng Q, Yan J, Stanciu G A, Welsch R E, So P T C, Csucs G and Yu H 2015 Experimenting liver fibrosis diagnostic by two photon excitation microscopy and bag-of-features image classification *Sci. Rep.* **4** 4636
- [105] Li L, Jiang W, Yang Y, Chen Z, Feng C, Li H, Guan G and Chen J 2014 Identification of dirty necrosis in colorectal carcinoma based on multiphoton microscopy *J. Biomed. Opt.* **19** 066008
- [106] Schueth A, van Zandvoort M A M J, Buurman W A and van Koeveringe G A 2014 Murine bladder imaging by 2-photon microscopy: an experimental study of morphology *J. Urol.* **192** 973–80
- [107] Yan J, Zhuo S, Chen G, Milsom J W, Zhang H, Lu J, Zhu W, Xie S, Chen J and Ying M 2014 Real-time optical diagnosis for surgical margin in low rectal cancer using multiphoton microscopy *Surg. Endosc.* **28** 36–41
- [108] Zhou Y, Kang D, Yang Z, Li L, Zhuo S, Zhu X, Zhou Y and Chen J 2016 Imaging normal and cancerous human gastric muscular layer in transverse and longitudinal sections by multiphoton microscopy: imaging the human gastric muscular layer by using MPM *Scanning* **38** 357–64
- [109] Skala M C, Squirrell J M, Vrotsos K M, Eickhoff J C, Gendron-Fitzpatrick A, Eliceiri K W and Ramanujam N 2005 Multiphoton autofluorescence of endogenous fluorescence differentiates normal, precancerous, and cancerous squamous epithelial tissues *Cancer Res.* **65** 1180–6
- [110] Matsui T et al 2017 Non-labeling multiphoton excitation microscopy as a novel diagnostic tool for discriminating normal tissue and colorectal cancer lesions *Sci. Rep.* **7** 6959
- [111] Sarri B et al 2019 Fast stimulated Raman and second harmonic generation imaging for intraoperative gastro-intestinal cancer detection *Sci. Rep.* **9** 10052
- [112] Li L, Kang D, Huang Z, Zhan Z, Feng C, Zhou Y, Tu H, Zhuo S and Chen J 2019 Multimodal multiphoton imaging for label-free monitoring of early gastric cancer *BMC Cancer* **19** 295
- [113] Shen B, Yan J, Wang S, Zhou F, Zhao Y, Hu R, Qu J and Liu L 2020 Label-free whole-colony imaging and metabolic analysis of metastatic pancreatic cancer by an autoregulating flexible optical system *Theranostics* **10** 1849–60
- [114] Zhang H, Chen Y, Cao D, Li W, Jing Y, Zhong H, Liu H and Zhu X 2021 Optical biopsy of laryngeal lesions using femtosecond multiphoton microscopy *Biomed. Opt. Express* **12** 1308
- [115] D'Hallewin M A, Baert L and Vanherzeele H 1994 *In vivo* fluorescence detection of human bladder carcinoma without sensitizing agents *J. Am. Paraplegia Soc.* **17** 161–4
- [116] Koenig F, McGovern F J, Althausen A F, Deutsch T F and Schomacker K T 1996 Laser induced autofluorescence diagnosis of bladder cancer *J. Urol.* **156** 1597–601
- [117] Zaak D, Stepp H, Baumgartner R, Schneede P, Waidelich R, Frimberger D, Hartmann A, Knchel R, Hofstetter A and Hohla A 2002 Ultraviolet-excited (308 nm) autofluorescence for bladder cancer detection *Urology* **60** 1029–33
- [118] Aboumarzouk O, Valentine R, Buist R, Ahmad S, Nabi G, Eljamel S, Moseley H and Kata S G 2015 Laser-induced autofluorescence spectroscopy: can it be of importance in detection of bladder lesions? *Photodiagn. Photodyn. Ther.* **12** 76–83
- [119] Kriegmair M C, Honeck P, Theuring M, Bolenz C and Ritter M 2018 Wide-field autofluorescence-guided TUR-B for the detection of bladder cancer: a pilot study *World J. Urol.* **36** 745–51
- [120] Anidjar M 1996 Ultraviolet laser-induced autofluorescence distinction between malignant and normal urothelial cells and tissues *J. Biomed. Opt.* **1** 335
- [121] Zheng W, Lau W, Cheng C, Soo K C and Olivo M 2003 Optimal excitation-emission wavelengths for autofluorescence diagnosis of bladder tumors *Int. J. Cancer* **104** 477–81
- [122] Mourant J R, Bigio I J, Boyer J, Conn R L, Johnson T and Shimada T 1995 Spectroscopic diagnosis of bladder cancer with elastic light scattering *Lasers Surg. Med.* **17** 350–7
- [123] Koenig F, Larne R, Enquist H, McGovern F J, Schomacker K T, Kollias N and Deutsch T F 1998 Spectroscopic measurement of diffuse reflectance for enhanced detection of bladder carcinoma *Urology* **51** 342–5
- [124] Slaton J, Hurst R, Davis C, Rajaputra P, You Y, Bartels K and Piao D 2016 MP61-09 early development of intravesical reflectance spectroscopy for bladder tumor detection and staging *J. Urol.* **195** e806
- [125] Rosenzweig B, Herr H and Coleman J A 2018 Narrow band imaging in the evaluation of upper tract urothelial cancer *Urothelial Malignancies of the Upper Urinary Tract* ed M Eshghi (Springer International Publishing) pp 129–43
- [126] Herr H W and Donat S M 2008 A comparison of white-light cystoscopy and narrow-band imaging cystoscopy to detect bladder tumour recurrences *BJU Int.* **102** 1111–4
- [127] Tatsugami K, Kuroiwa K, Kamoto T, Nishiyama H, Watanabe J, Ishikawa S, Shinohara N, Sazawa A, Fukushima S and Naito S 2010 Evaluation of narrow-band imaging as a complementary method for the detection of bladder cancer *J. Endourol.* **24** 1807–11
- [128] Chen G, Wang B, Li H, Ma X, Shi T and Zhang X 2013 Applying narrow-band imaging in complement with white-light imaging cystoscopy in the detection of urothelial carcinoma of the bladder *Urol. Oncol.* **31** 475–9

- [129] Ye Z *et al* 2015 A comparison of NBI and WLI cystoscopy in detecting non-muscle-invasive bladder cancer: a prospective, randomized and multi-center study *Sci. Rep.* **5** 10905
- [130] Crow P, Uff J S, Farmer J A, Wright M P and Stone N 2004 The use of Raman spectroscopy to identify and characterize transitional cell carcinoma in vitro *BJU Int.* **93** 1232–6
- [131] Crow P, Molckovsky A, Stone N, Uff J, Wilson B and WongKeeSong L-M 2005 Assessment of fiberoptic near-infrared raman spectroscopy for diagnosis of bladder and prostate cancer *Urology* **65** 1126–30
- [132] Draga R O P, Grimbergen M C M, Vijverberg P L M, Swol C F P V, Jonges T G N, Kummer J A and Ruud Bosch J L H 2010 *In vivo* bladder cancer diagnosis by high-volume Raman spectroscopy *Anal. Chem.* **82** 5993–9
- [133] Barman I, Dingari N C, Singh G P, Kumar R, Lang S and Nabi G 2012 Selective sampling using confocal Raman spectroscopy provides enhanced specificity for urinary bladder cancer diagnosis *Anal. Bioanal. Chem.* **404** 3091–9
- [134] Cordero E, Ruger J, Marti D, Mondol A S, Hasselager T, Mogensen K, Hermann G G, Popp J and Schie I W 2020 Bladder tissue characterization using probe-based Raman spectroscopy: evaluation of tissue heterogeneity and influence on the model prediction *J. Biophoton.* **13** e201960025
- [135] Placzek F *et al* 2020 Morpho-molecular *ex vivo* detection and grading of non-muscle-invasive bladder cancer using forward imaging probe based multimodal optical coherence tomography and Raman spectroscopy *Analyt.* **145** 1445–56
- [136] Chen H, Li X, Broderick N, Liu Y, Zhou Y, Han J and Xu W 2018 Identification and characterization of bladder cancer by low-resolution fiber-optic Raman spectroscopy *J. Biophoton.* **11** e201800016
- [137] de Jong B W D, Bakker Schut T C, Maquelin K, van der Kwast T, Bangma C H, Kok D-J and Puppels G J 2006 Discrimination between nontumor bladder tissue and tumor by Raman spectroscopy *Anal. Chem.* **78** 7761–9
- [138] Mukherjee S, Wysock J S, Ng C K, Akhtar M, Perner S, Lee M-M, Rubin M A, Maxfield F R, Webb W W and Scherr D S 2009 Human bladder cancer diagnosis using multiphoton microscopy *Proc. SPIE* **7161** 716117
- [139] Cicchi R, Crisci A, Cosci A, Nesi G, Kapsokalyvas D, Giancane S, Carini M and Pavone F S 2010 Time- and Spectral-resolved two-photon imaging of healthy bladder mucosa and carcinoma in situ *Opt. Express* **18** 3840
- [140] Jain M, Robinson B D, Shevchuk M M, Aggarwal A, Salamoon B, Dubin J M, Scherr D S and Mukherjee S 2015 Multiphoton microscopy: a potential intraoperative tool for the detection of carcinoma *in situ* in human bladder *Arch. Pathol. Lab. Med.* **139** 796–804
- [141] Katz M J, Huland D M and Ramasamy R 2014 Multiphoton microscopy: applications in urology and andrology *Transl. Androl. Urol.* **3** 77–83
- [142] Marchetti M, Baria E, Cicchi R and Pavone F S 2019 Custom multiphoton/raman microscopy setup for imaging and characterization of biological samples *Methods Protocols* **2** 51
- [143] Jain M *et al* 2012 Multiphoton microscopy in the evaluation of human bladder biopsies *Arch. Pathol. Lab. Med.* **136** 517–26
- [144] Baria E, Barone A, Nesi G, Pavone F S and Cicchi R Imaging of human urothelial carcinoma samples using multimodal multiphoton microscopy *European Conf. on Biomedical Optics (Munich, Germany, 28 July 2017)* p 104140Q
- [145] Frangioni J 2003 *In vivo* near-infrared fluorescence imaging *Curr. Opin. Chem. Biol.* **7** 626–34
- [146] Lim Y T, Kim S, Nakayama A, Stott N E, Bawendi M G and Frangioni J V 2003 Selection of quantum dot wavelengths for biomedical assays and imaging *Mol. Imaging* **2** 50–64
- [147] Lefort C 2017 A review of biomedical multiphoton microscopy and its laser sources *J. Phys. D: Appl. Phys.* **50** 423001
- [148] Weber M J 1999 *Handbook of Laser Wavelengths* (CRC Press)
- [149] Okhotnikov O G 2012 *Fiber Lasers* (Wiley-VCH Verlag GmbH)
- [150] Denker B and Shklovsky E 2013 *Handbook of Solid-state Lasers: Materials, Systems and Applications* (Elsevier)
- [151] Poudel C and Kaminski C F 2019 Supercontinuum radiation in fluorescence microscopy and biomedical imaging applications *J. Opt. Soc. Am. B* **36** A139–53
- [152] Harreguy M B, Marfil V, Grooms N W F, Gabel C V, Chung S H and Haspel G 2020 Ytterbium-doped fibre femtosecond laser offers robust operation with deep and precise microsurgery of *C. elegans* neurons *Sci. Rep.* **10** 4545
- [153] Zhao Y, Nakamura H and Gordon R J 2010 Development of a versatile two-photon endoscope for biological imaging *Biomed. Opt. Express* **1** 1159
- [154] Rivera D R, Brown C M, Ouzounov D G, Pavlova I, Kobat D, Webb W W and Xu C 2011 Compact and flexible raster scanning multiphoton endoscope capable of imaging unstained tissue *Proc. Natl Acad. Sci.* **108** 17598–603
- [155] Brown C M, Rivera D R, Pavlova I, Ouzounov D G, Williams W O, Mohanan S, Webb W W and Xu C 2012 *In vivo* imaging of unstained tissues using a compact and flexible multiphoton microendoscope *J. Biomed. Opt.* **17** 040505
- [156] Liang W, Murari K, Zhang Y, Chen Y, Li M-J and Li X 2012 Increased illumination uniformity and reduced photodamage offered by the Lissajous scanning in fiber-optic two-photon endomicroscopy *J. Biomed. Opt.* **17** 021108
- [157] Huland D M, Brown C M, Howard S S, Ouzounov D G, Pavlova I, Wang K, Rivera D R, Webb W W and Xu C 2012 *In vivo* imaging of unstained tissues using long gradient index lens multiphoton endoscopic systems *Biomed. Opt. Express* **3** 1077
- [158] Xi J, Chen Y, Zhang Y, Murari K, Li M-J and Li X 2012 Integrated multimodal endomicroscopy platform for simultaneous en face optical coherence and two-photon fluorescence imaging *Opt. Lett.* **37** 362
- [159] Liang W, Hall G, Messerschmidt B, Li M-J and Li X 2017 Nonlinear optical endomicroscopy for label-free functional histology *in vivo Light Sci. Appl.* **6** e17082
- [160] Lombardini A *et al* 2018 High-resolution multimodal flexible coherent Raman endoscope *Light Sci. Appl.* **7** 10
- [161] Dilipkumar A *et al* 2019 Label-free multiphoton endomicroscopy for minimally invasive *in vivo* imaging *Adv. Sci.* **6** 1801735
- [162] Ouzounov D G, Rivera D R, Williams W O, Stupinski J A, Southard T L, Hume K H, Bentley J, Weiss R S, Webb W W and Xu C 2013 Dual modality endomicroscope with optical zoom capability *Biomed. Opt. Express* **4** 1494
- [163] Lefort C, Hamzeh H, Louradour F, Pain F and Haidar D A 2014 Characterization, comparison, and choice of a commercial double-clad fiber for nonlinear endomicroscopy *J. Biomed. Opt.* **19** 076005
- [164] Ducourthial G *et al* 2015 Development of a real-time flexible multiphoton microendoscope for label-free imaging in a live animal *Sci. Rep.* **5** 18303
- [165] Hamzeh H, Lefort C, Pain F and Haidar D 2015 Optimization and characterization of nonlinear excitation and collection through a gradient-index lens for high-resolution nonlinear endomicroscopy *Opt. Lett.* **40** 808
- [166] Kim Y, Warren S C, Stone J M, Knight J C, Neil M A A, Paterson C, Dunsby C W and French P M W 2016 Adaptive multiphoton endomicroscope incorporating a polarization-maintaining multicore optical fibre *IEEE J. Sel. Top. Quantum Electron.* **22** 171–8
- [167] Pshenay-Severin E *et al* 2021 Multimodal nonlinear endomicroscopic imaging probe using a double-core double-clad fiber and focus-combining micro-optical concept *Light Sci. Appl.* **10** 207



- [168] Sordillo L A, Pu Y, Pratavieira S, Budansky Y and Alfano R R 2014 Deep optical imaging of tissue using the second and third near-infrared spectral windows *J. Biomed. Opt.* **19** 056004
- [169] Tomilov S, Wang Y, Hoffmann M, Heidrich J, Golling M, Keller U and Saraceno C J 2022 50-W average power Ho:YAG SESAM-modelocked thin-disk oscillator at 2.1  $\mu\text{m}$  *Opt. Express* **30** 27662–73
- [170] Li P, Ruehl A, Grosse-Wortmann U and Hartl I 2014 Sub-100 fs passively mode-locked holmium-doped fiber oscillator operating at 2.06  $\mu\text{m}$  *Opt. Lett.* **39** 6859–62
- [171] Rudy C W, Digonnet M J and Byer R L 2014 Advances in 2- $\mu\text{m}$  Tm-doped mode-locked fiber lasers *Opt. Fiber Technol.* **20** 642–9
- [172] Kamynin V A, Filatova S A, Denker B I, Galagan B I, Koltashev V V, Medvedkov O I, Sverchkov S and Tsvetkov V B 2021  $\text{Tm}^{3+}$ -doped tellurite fiber weak signal amplifier at a wavelength of 2.27  $\mu\text{m}$  *Results Phys.* **27** 104512
- [173] Sordillo D C, Sordillo L A, Sordillo P P, Shi L and Alfano R R 2017 Short wavelength infrared optical windows for evaluation of benign and malignant tissues *J. Biomed. Opt.* **22** 045002
- [174] Yamanaka M, Teranishi T, Kawagoe H and Nishizawa N 2016 Optical coherence microscopy in 1700 nm spectral band for high-resolution label-free deep-tissue imaging *Sci. Rep.* **6** 31715
- [175] Sordillo L A, Pratavieira S, Pu Y, Salas-Ramirez K, Shi L, Zhang L, Budansky Y and Alfano R R 2014 Third therapeutic spectral window for deep tissue imaging *Proc. SPIE* **8940** 89400V
- [176] Helmchen F and Denk W 2005 Deep tissue two-photon microscopy *Nat. Methods* **2** 932–40
- [177] Xu L, Feehan J S, Shen L, Peacock A C, Shepherd D P, Richardson D J and Price J H V 2014 Yb-fiber amplifier pumped idler-resonant PPLN optical parametric oscillator producing 90 femtosecond pulses with high beam quality *Appl. Phys. B* **117** 987–93
- [178] Krauth J, Steinmann A, Hegenbarth R, Conforti M and Giessen H 2013 Broadly tunable femtosecond near- and mid-IR source by direct pumping of an OPA with a 417 MHz Yb:KGW oscillator *Opt. Express* **21** 11516
- [179] Fan J, Gu C, Zhao J, Liao R, Chu Y, Chai L, Wang C and Hu M 2018 Dielectric-mirror-less femtosecond optical parametric oscillator with ultrabroad-band tunability *Opt. Lett.* **43** 2316
- [180] Kiani L, Lu T and Sharping J E 2014 Comparison of amplitude noise of a fiber-optical parametric oscillator and a supercontinuum source *J. Opt. Soc. Am. B* **31** 1986
- [181] O'Connor M V, Watson M A, Shepherd D P, Hanna D C, Price J H V, Malinowski A, Nilsson J, Broderick N G R, Richardson D J and Lefort L 2002 Synchronously pumped optical parametric oscillator driven by a femtosecond mode-locked fiber laser *Opt. Lett.* **27** 1052
- [182] Mörz F, Steinle T, Steinmann A and Giessen H 2015 Multi-Watt femtosecond optical parametric master oscillator power amplifier at 43 MHz *Opt. Express* **23** 23960
- [183] Steinle T, Mörz F, Steinmann A and Giessen H 2016 Ultra-stable high average power femtosecond laser system tunable from 133 to 20  $\mu\text{m}$  *Opt. Lett.* **41** 4863
- [184] Tzeng Y-W, Huang C-H, Lin Y-Y, Liu J-M, Chui H-C, Liu H-L, Stone J M, Knight J C and Chu S-W 2009 High repetition rate optical parametric amplification based on a single Yb: fiber laser *Conf. on Lasers and Electro-Optics/Int. Quantum Electronics Conf. p CWJ7*
- [185] Rigaud P, Van de Walle A, Hanna M, Forget N, Guichard F, Zaouter Y, Guesmi K, Druon F and Georges P 2016 Supercontinuum-seeded few-cycle mid-infrared OPCPA system *Opt. Express* **24** 26494
- [186] Kanai T, Lee Y, Seo M and Kim D E 2019 Supercontinuum-seeded, carrier-envelope phase-stable, 45-W, 38- $\mu\text{m}$ , 6-cycle, KTA optical parametric amplifier driven by a 14-ps Yb:YAG thin-disk amplifier for nonperturbative spectroscopy in solids *J. Opt. Soc. Am. B* **36** 2407
- [187] Becheker R, Tang M, Hanzard P-H, Tyazhev A, Mussot A, Kudlinski A, Kellou A, Oudar J-L, Godin T and Hideur A 2018 High-energy dissipative soliton-driven fiber optical parametric oscillator emitting at 1.7  $\mu\text{m}$  *Laser Phys. Lett.* **15** 115103
- [188] Hanna M, Druon F and Georges P 2006 Fiber optical parametric chirped-pulse amplification in the femtosecond regime *Opt. Express* **14** 2783
- [189] Cristofori V, Lali-Dastjerdi Z, Rishøj L S, Galili M, Peucheret C and Rottwitz K 2013 Dynamic characterization and amplification of sub-picosecond pulses in fiber optical parametric chirped pulse amplifiers *Opt. Express* **21** 26044
- [190] Qin Y, Batjargal O, Cromey B and Kieu K 2020 High-power 1700 nm femtosecond laser based on optical parametric chirped-pulse amplification *Conf. on Lasers and Electro-Optics p STh1P.5*
- [191] Qin Y, Batjargal O, Cromey B and Kieu K 2020 All-fiber high-power 1700 nm femtosecond laser based on optical parametric chirped-pulse amplification *Opt. Express* **28** 2317
- [192] Roy R, Schulz P A and Walther A 1987 Acousto-optic modulator as an electronically selectable unidirectional device in a ring laser *Opt. Lett.* **12** 672
- [193] Yang K, Zhao P, Luo J, Huang K, Hao Q and Zeng H 2018 Comparison on different repetition rate locking methods in Er-doped fiber laser *Laser Phys.* **28** 055108
- [194] Korobko D A, Stoliarov D A, Itrin P A, Odnoblyudov M A, Petrov A B and Gumenyuk R V 2021 Harmonic mode-locking fiber ring laser with a pulse repetition rate up to 12 GHz *Opt. Laser Technol.* **133** 106526
- [195] Stoliarov D A, Itrin P A, Ribenek V A, Korobko D A and Fotiadi A A 2020 Linear cavity fiber laser harmonically mode-locked with SESAM *Laser Phys. Lett.* **17** 105102
- [196] Ribenek V A, Stoliarov D A, Korobko D A and Fotiadi A A 2021 Mitigation of the supermode noise in a harmonically mode-locked ring fiber laser using optical injection *Opt. Lett.* **46** 5747–50
- [197] Khagai A, Melkumov M, Riumkin K, Khopin V, Firstov S and Dianov E 2018 NALM-based bismuth-doped fiber laser at 1.7  $\mu\text{m}$  *Opt. Lett.* **43** 1127
- [198] Fujimoto Y and Nakatsuka M 2001 Infrared luminescence from bismuth-doped silica glass *Jpn. J. Appl. Phys.* **40** L279–81
- [199] Noronen T, Melkumov M, Stolyarov D, Khopin V F, Dianov E and Okhotnikov O G 2015 All-bismuth fiber system for femtosecond pulse generation, compression, and energy scaling *Opt. Lett.* **40** 2217
- [200] Firstov S V, Alyshev S V, Riumkin K E, Khagai A M, Kharakhordin A V, Melkumov M A and Dianov E M 2018 Laser-active fibers doped with bismuth for a wavelength region of 1.6–1.8  $\mu\text{m}$  *IEEE J. Sel. Top. Quantum Electron.* **24** 1–15
- [201] Noronen T, Firstov S, Dianov E and Okhotnikov O G 2016 1700 nm dispersion managed mode-locked bismuth fiber laser *Sci. Rep.* **6** 24876
- [202] Emami S D, Dashtabi M M, Lee H J, Arabanian A S and Rashid H A A 2017 1700 nm and 1800 nm band tunable thulium doped mode-locked fiber lasers *Sci. Rep.* **7** 12747
- [203] Liu X, Sahu J K and Gumenyuk R 2023 Tunable dissipative soliton Tm-doped fiber laser operating from 1700 nm to 1900 nm *Opt. Lett.* **48** 612–5

- [204] Stolen R and Lin C 1978 Self-phase-modulation in silica optical fibers *Phys. Rev. A* **17** 1448
- [205] Islam M N, Simpson J R, Shang H T, Mollenauer L F and Stolen R H 1987 Cross-phase modulation in optical fibers *Opt. Lett.* **12** 625
- [206] Stolen R 1975 Phase-matched-stimulated four-photon mixing in silica-fiber waveguides *IEEE J. Quantum Electron.* **11** 100–3
- [207] Eckhardt G, Bortfeld D P and Geller M 1963 Stimulated emission of Stokes and anti-Stokes Raman lines from diamond, calcite, and  $\alpha$ -sulfur single crystals *Appl. Phys. Lett.* **3** 137–8
- [208] Smith R G 1972 Optical power handling capacity of low loss optical fibers as determined by stimulated raman and brillouin scattering *Appl. Opt.* **11** 2489
- [209] Chiao R Y, Townes C H and Stoicheff B P 1964 Stimulated brillouin scattering and coherent generation of intense hypersonic waves *Phys. Rev. Lett.* **12** 592–5
- [210] Ippen E P 1970 Low-power quasi-cw Raman oscillator *Appl. Phys. Lett.* **16** 303–5
- [211] Agrawal G P 2011 Nonlinear fiber optics: its history and recent progress *J. Opt. Soc. Am. B* **28** A1
- [212] He X, Lin Q, Guo H, Sun J, Bai J, Hou L and Wang K 2019 Robust 1.7- $\mu\text{m}$ , all-polarization-maintaining femtosecond fiber laser source based on standard telecom fibers *Appl. Phys. Express* **12** 072007
- [213] Fang X, Wang Z and Zhan L 2017 Efficient generation of all-fiber femtosecond pulses at 1.7  $\mu\text{m}$  via soliton self-frequency shift *Opt. Eng.* **56** 046107
- [214] Chung H Y, Liu W, Cao Q, Kärtner F X and Chang G 2017 Er-fiber laser enabled, energy scalable femtosecond source tunable from 1.3 to 1.7  $\mu\text{m}$  *Opt. Express* **25** 15760–71
- [215] Cadroas P et al 2017 All-fiber femtosecond laser providing 9 nJ, 50 MHz pulses at 1650 nm for three-photon microscopy *J. Opt.* **19** 065506
- [216] Stoliarov D, Koviárov A, Korobko D, Galiakhmetova D and Rafailov E 2022 Fibre laser system with wavelength tuning in extended telecom range *Opt. Fiber Technol.* **72** 102994
- [217] Wang K, Horton N G, Charan K and Xu C 2014 Advanced fiber soliton sources for nonlinear deep tissue imaging in biophotonics *IEEE J. Sel. Top. Quantum Electron.* **20** 6800311
- [218] Zanoni M, Piccinini F, Arienti C, Zamagni A, Santi S, Polico R, Bevilacqua A and Tesi A 2016 3D tumor spheroid models for in vitro therapeutic screening: a systematic approach to enhance the biological relevance of data obtained *Sci. Rep.* **6** 19103
- [219] Zanoni M, Cortesi M, Zamagni A, Arienti C, Pignatta S and Tesi A 2020 Modeling neoplastic disease with spheroids and organoids *J. Hematol. Oncol.* **13** 97
- [220] Kastner C, Hendricks A, Deinlein H, Hankir M, Germer C-T, Schmidt S and Wiegner A 2021 Organoid models for cancer research—from bed to bench side and back *Cancers* **13** 4812
- [221] Sachs N et al 2018 A living biobank of breast cancer organoids captures disease heterogeneity *Cell* **172** 373–86.e10
- [222] Atat O E, Farzaneh Z, Pourhamzeh M, Taki F, Abi-Habib R, Vosough M and El-Sibai M 2022 3D modeling in cancer studies *Hum. Cell* **35** 23–36
- [223] Palmer S, Litvinova K, Dunaev A, Fleming S, McGloin D and Nabi G 2016 Changes in autofluorescence based organoid model of muscle invasive urinary bladder cancer *Biomed. Opt. Express* **7** 1193–200
- [224] Banerjee S and Southgate J 2019 Bladder organoids: a step towards personalised cancer therapy? *Transl. Androl. Urol.* **8** S300–2
- [225] Seidlitz T and Stange D E 2021 Gastrointestinal cancer organoids—applications in basic and translational cancer research *Exp. Mol. Med.* **53** 1459–70
- [226] Zhang R et al 2021 Development and application of patient-derived cancer organoids in clinical management of gastrointestinal cancer: a state-of-the-art review *Front. Oncol.* **11** 716339
- [227] Yoshida T, Sopko N A, Kates M, Liu X, Joice G, Mcconkey D J and Bivalacqua T J 2019 Impact of spheroid culture on molecular and functional characteristics of bladder cancer cell lines *Oncol. Lett.* **18** 4923–9
- [228] Kim H, Han Y, Suhito I R, Choi Y, Kwon M, Son H, Kim H-R and Kim T-H 2021 Raman spectroscopy-based 3D analysis of odontogenic differentiation of human dental pulp stem cell spheroids *Anal. Chem.* **93** 9995–10004
- [229] Gil D A, Deming D and Skala M C 2021 Patient-derived cancer organoid tracking with wide-field one-photon redox imaging to assess treatment response *J. Biomed. Opt.* **26** 036005
- [230] Pasquale V, Ducci G, Campioni G, Ventrici A, Assalini C, Busti S, Vanoni M, Vago R and Sacco E 2020 Profiling and targeting of energy and redox metabolism in grade 2 bladder cancer cells with different invasiveness properties *Cells* **9** E2669
- [231] Walsh A J, Cook R S and Skala M C 2017 Functional optical imaging of primary human tumor organoids: development of a personalized drug screen *J. Nucl. Med.* **58** 1367–72
- [232] Hu L-F, Yang X, Lan H-R, Fang X-L, Chen X-Y and Jin K-T 2021 Preclinical tumor organoid models in personalized cancer therapy: not everyone fits the mold *Exp. Cell. Res.* **408** 112858
- [233] Wang L, Fan J-H, Guan Z-F, Liu Y, Zeng J, He D-L, Huang L-Q, Wang X-Y and Gong H-L 2012 Study on bladder cancer tissues with Raman spectroscopy *Guang Pu* **32** 123–6
- [234] Bovenkamp D et al 2018 Combination of high-resolution optical coherence tomography and raman spectroscopy for improved staging and grading in bladder cancer *Appl. Sci.* **8** 2371